TITLE PAGE

Mechanistic Evaluation of the Complex Drug-Drug Interactions of Maraviroc: Contribution of Cytochrome P450 3A, P-Glycoprotein and Organic Anion Transporting Polypeptide 1B1

Emi Kimoto, Manoli Vourvahis, Renato J. Scialis, Heather Eng, A. David Rodrigues, Manthena V. S. Varma

Pharmacokinetics, Pharmacodynamics and Metabolism, Medicine Design, Pfizer Inc., Groton, CT, USA (EK, RJS[#], HE, ADR, MVSV); and Clinical Pharmacology, Pfizer Inc., New York, NY, USA (MV)

[#]Current affiliation: Metabolism and Pharmacokinetics, Preclinical Candidate Optimization, Bristol-Myers Squibb, Princeton, NJ, USA

RUNNING TITLE PAGE

Running Title: Mechanistic Evaluation of Maraviroc DDIs

Correspondence to:

Emi Kimoto, Ph.D.

Pharmacokinetics, Dynamics, and Metabolism, Medicine Design, Pfizer Inc.

Eastern Point Road, Groton, CT 06340.

Tel: 860-686-9562

Fax: 860-686-5364

E-mail: emi.kimoto@pfizer.com

Manuscript Metrics:

Number of text pages: 37

Number of tables: 5

Number of figures: 5

Number of references: 63

Number of words in the Abstract: 237 words

Number of words in the Introduction: 557 words

Number of words in the Discussion: 1633 words

ABBREVIATIONS:

ANOVA, one-way analysis of variance; ATP, adenosine triphosphate; AUC, area under the concentration-time curve; CI, confidence interval; C_{max}, maximum plasma concentration; CYP, cytochrome P450; DDI, drug-drug interaction; Fa, fraction of the dose absorbed from gastrointestinal tract; Fg, fraction of the dose that escapes intestinal first-pass metabolism; Fh, fraction of the dose that escapes hepatic first-pass metabolism; f_u, unbound fraction; MRM, multiple reaction monitoring; MRP, multidrug resistance-associated protein; MVC, maraviroc; OATP, physiologically-based pharmacokinetic; PBPK, organic anion transporting polypeptide; SCHH, sandwich-cultured human hepatocytes; SLC, solute carrier; TDI, time-dependent inhibition; TVR, telaprevir; UGT, UDP-glucuronosyltransferase;

ABSTRACT

The aim of the present study was to quantitatively evaluate the drug-drug interactions (DDIs) of maraviroc (MVC) with various perpetrator drugs, including telaprevir (TVR), using *in vitro* data-informed physiologically based pharmacokinetic (PBPK) model. MVC showed significant active uptake and biliary excretion in sandwich-cultured human hepatocytes, and two-K_m organic anion transporting polypeptide (OATP)1B1-mediated uptake in transfected cells (high-affinity K_m ~5 μM). No measureable active uptake was noted in OATP1B3- and OATP2B1-transfceted cells. TVR inhibited OATP1B1-mediated MVC transport *in vitro*, and also exhibited CYP3A time-dependent inhibition (TDI) in human hepatocytes (inactivation constant, K_I = 2.24 μM, and maximum inactivation rate constant, k_{inact} = 0.0112 min^{-1}). The inactivation efficiency (k_{inact}/K_I) was approximately 34-fold lower in human hepatocytes compared to liver microsomes. A PBPK model accounting for interactions involving CYP3A, P-glycoprotein (P-gp), and OATP1B1 was developed based on *in vitro* mechanistic data. MVC DDIs with ketoconazole (inhibition of CYP3A and P-gp), ritonavir (inhibition of CYP3A and P-gp), efavirenz (induction of CYP3A), rifampicin (induction of CYP3A and P-gp; inhibition of OATP1B1) and TVR (inhibition of CYP3A, P-gp, and OATP1B1) were well described by the PBPK model with optimized transporter K_i values implying that OATP1B1-mediated uptake, along with CYP3A metabolism, determines the hepatic clearance of MVC; and P-gp-mediated efflux limits its intestinal absorption. In summary, MVC disposition involves intestinal P-gp/CYP3A and hepatic OATP1B1/CYP3A interplay; and TVR simultaneously inhibits these multiple mechanisms leading to a strong DDI – about 9.5-fold increase in MVC oral exposure.

INTRODUCTION

Drug-drug interactions (DDIs) involving drug-metabolizing enzymes and membrane transporters can lead to changes in victim drug exposure, which can result in adverse effects and impact efficacy. Therefore, it is important to evaluate potential DDIs in drug discovery and during clinical development, as reflected in the guidance documents provided by various health authorities (Committee for Human Medicinal Products (CHMP), 2012; The Japanese Ministry of Health, 2014; Center for Drug Evaluation and Research (CDER), 2017). While successful approaches have been developed to predict DDIs involving cytochrome P450 enzyme (CYP) inhibition or induction in isolation, the optimal strategy to evaluate complex DDIs such as mixed enzyme inhibition-induction or combined competitive and time-dependent inhibition (TDI) or simultaneous transporter-enzyme interactions continue to evolve (Fahmi et al., 2009; Vieira et al., 2014; Varma et al., 2015; Wagner et al., 2015).

Maraviroc (MVC) is a selective C-C chemokine receptor type 5 (CCR5) antagonist approved for the treatment of human immunodeficiency virus (HIV) infection (Abel et al., 2009). MVC is primarily metabolized by CYP3A with renal clearance accounting for about 23% of total clearance; and is a substrate of P-glycoprotein (P-gp) and organic anion transporting polypeptide (OATP)1B1 (Walker et al., 2005; Hyland et al., 2008; Siccardi et al., 2010). MVC exposure was shown to increase significantly when co-administered with strong CYP3A/P-gp inhibitors in humans (Hyland et al., 2008). Clinical studies also indicated that the mean area under the plasma concentration-time curve (AUC) of MVC increased by approximately 9.5-fold when treated with telaprevir (TVR) (Vourvahis et al., 2014). The magnitude of this interaction is much greater than that observed with other strong CYP3A probe inhibitors (e.g. 2.5-fold with ritonavir to 5-fold with ketoconazole) (Abel et al., 2008b; Vourvahis et al., 2014). Earlier studies showed an association between MVC plasma trough concentrations and the *SLCO1B1* 521TC genotype in patients treated with 60 mg plus etravirine or efavirenz (Siccardi et al., 2010). More recent genotype-

pharmacokinetic analyses have shown that homozygous or heterozygous carriers of the *SLCO1B1* 521T>C allele are characterized by higher MVC exposure (AUC_{0-12}, C_{max}, and C_{min}) versus reference TT homozygote subjects (Vourvahis et al., 2011). These clinical findings indicate that OATP1B1 plays a significant role in the hepatic clearance of MVC. HIV infected patients are likely to be at risk for other infectious pathogens, including hepatitis B virus (HBV) or hepatitis C virus (HCV). For example, the results of a recent meta-analysis study indicated more than 2 million people are co-infected with HIV and HCV globally (Platt et al., 2016). Although use of TVR, a direct-acting antiviral for the treatment of genotype 1 chronic HCV patients, has been discontinued, a number of DDIs were reported which may involve inhibition of not only CYP3A but also P-gp and OATP1B1.

The aim of this study was to quantitatively evaluate MVC pharmacokinetic interactions based on mechanistic *in vitro* studies and physiologically based pharmacokinetic (PBPK) modeling and simulations. First, transporter-mediated disposition of MVC was characterized *in vitro* using transfected cells and primary human hepatocytes. Secondly, a permeability-limited hepatic disposition model was considered in the PBPK analyses, and verified using a range of available clinical DDI data with various perpetrator drugs including ketoconazole, ritonavir, efavirenz, rifampicin, and with TVR, which caused up to 9.5-fold increase in MVC plasma exposure. Prior to this, TVR perpetrator model was verified using DDI data with probe substrate drugs – midazolam (CYP3A), digoxin (P-gp) and atorvastatin (CYP3A/P-gp/OATP1B1).

MATERIALS AND METHODS

Materials and Reagents. In VitroGro-HT (thawing), In VitroGro-CP (plating), and In VitroGro-HI (incubation) hepatocyte media were purchased from Celsis In Vitro Technologies Inc. (IVT) (Baltimore, MD). Hanks balanced salt solution (HBSS) Ca^{2+}/Mg^{2+}-containing (standard) was purchased from Lonza (Walkersville, MD), and HBSS Ca^{2+}/Mg^{2+}-free and William's medium E were purchased from Gibco (Grand Island, NY). BioCoat 24-well plates and Matrigel^{TM} were purchased from Corning (Kennebunk, ME). The BCA Protein Assay Kit was purchased from PierceBiotechnology (Rockford, IL). HPLC grade methanol, acetonitrile, and water were obtained from Fisher Chemical (Fair Lawn, NJ). TPV was purchased from Toronto Research Chemicals Inc. (ON, Canada). Midazolam was purchased from United States Pharmacopeia (Rockville, MD), and 1'-hydroxymidazolam and D4-1'-hydroxymidazolam were synthesized at Pfizer Inc. MVC, formic acid, dulbecco's phosphate-buffer saline, Krebs-Henseleit buffer, monobasic and dibasic potassium phosphate buffer, magnesium chloride, HEPES, reduced nicotinamide adenine dinucleotide phosphate (NADPH), and all other chemicals were purchased from Sigma-Aldrich (St. Louis, MO). Cryopreserved human hepatocyte lot HU4241 (male, Caucasian, age 53) was purchased from Invitrogen (Waltham, MA) and HH1025 (female, Caucasian, age 59) was purchased from In Vitro ADMET (Columbia, MD). Pooled male and female human liver microsomes (n = 50 donors) were purchased from Sekisui Xenotech (Kansas City, KS), and pooled male and female hepatocytes (n = 10 donors) were purchased from Bioreclamation IVT (Baltimore, MD).

Transport studies in Sandwich-Cultured Human Hepatocytes (SCHH). Plateable cryopreserved hepatocytes were thawed and plated as described previously (Kimoto et al., 2015). Briefly, hepatocytes were thawed in a water bath at 37°C and placed on ice. The cells were then poured into In VitroGro-HT medium at 37°C at a ratio of one vial/50 mL in a conical tube. The cells were centrifuged at 50 × g for 3 min and resuspended at 0.75 × 10^6 cells/mL in In VitroGro-CP medium. Cell viability was determined by

trypan blue exclusion and exceeded 85%. On day 1, hepatocyte suspensions were plated in collagen-

coated 24-well plates at a density of 0.375×10^6 cells/well in a volume of 0.5 mL/well. After 18 to 24 hours

of incubation at 37°C, cells were overlaid with ice-cold 0.25 mg/mL Matrigel™ in In VitroGro-HI medium

at 0.5 mL/well. Cultures were maintained in In VitroGro-HI medium that was refreshed every 24 hours.

On day 5 of SCHH, the hepatocytes were first rinsed twice with Ca^{2+}/Mg^{2+}-containing (standard) or

Ca^{2+}/Mg^{2+}-free HBSS, and then pre-incubated for 10 min with standard or Ca^{2+}/Mg^{2+}-free HBSS in the

absence or presence of inhibitors at 37°C or 4°C. After aspirating the pre-incubation buffer, 0.5 mL of

incubation buffer containing substrate was added in the absence or presence of inhibitors at 37°C or 4°C.

The uptake was terminated at a designated time (0.5, 1, 2, 5, 10 and 15 min) by adding 0.5 mL of ice cold

standard HBSS after removal of the incubation buffer. Cells were then washed three times with 0.5 mL of

ice cold standard HBSS. The hepatocytes were lysed with methanol containing the internal standard for

LC-MS/MS quantification (Supplemental Methods).

Transport studies in Suspended Human Hepatocytes. Uptake of MVC was measured using

suspended human hepatocytes as described previously (Kimoto et al., 2011; Bi et al., 2013). Briefly,

cryopreserved hepatocytes were thawed at 37°C and then immediately suspended in In VitroGro-HT

medium. The hepatocytes were centrifuged at $50 \times g$ for 3 min at room temperature, and the cells were

resuspended in Krebs-Henseleit buffer. Cell viability was determined by trypan blue exclusion and

exceeded 85%. The hepatocytes were diluted to 2×10^6 cells/mL. An aliquot of cells (200 μL) was placed

in test tubes and prewarmed in a slow-motion 37°C water bath or ice-cold bath for 3 min. Uptake

incubations were initiated by the addition of 200 μL of MVC (2 μM) pre-warmed (37°C) or ice-cold, which

resulted a final substrate concentration of 1 μM and a cell density of 1×10^6 cells/mL in a 400 μL incubation

volume. The incubations were terminated at 0.5, 1, and 1.5 min by collection of 100 μL of incubation

mixture into a centrifuge tube that was previously prepared with two layers: a bottom layer of 50 μL of

2N NaOH and an upper layer of 100 μL oil (density = 1.015; a mixture of silicone oil and mineral oil). The

tube was immediately centrifuged at 16,000 × g for 10 sec (Microfuge E; Beckman Coulter, Fullerton, CA).

The centrifuge tubes were cut at the middle of the oil layer to separate the bottom layer containing cells.

Ammonium acetate in the bottom layer was aspirated and the cell pellets were transferred to a 96 well

plate after re-suspending with 50 µL of water. The cells were lysed with 100 µL of methanol containing

internal standard. The concentrations of analytes were determined by LC-MS/MS in Supplemental

Methods.

Transport Studies in Transfected HEK293 Cells. OATP1B1, OATP1B3, and OATP2B1 specific

transport was assessed in stably-transfected human embryonic kidney (HEK293) cells. Transporter-

transfected and wild-type HEK293 cells were seeded onto 24-, 48- or 98-well poly-D-lysine-coated plates

at a density of 2×10^5 cells (24 well) per well in a total volume of 0.5 mL per well, 1.125×10^5 cells (48

well) per well in a total volume of 0.25 mL per well or 2.5 to 5×10^4 cells per well in a total volume of 0.1

mL per well (96-well). OATP-transfected cells were cultured for 48-72 hours in the presence of Dulbecco's

modified Eagle medium, 10% heat-inactivated fetal bovine serum, and 5 µg/mL blasticidin. After the cells

reached confluency, they were washed two times with uptake buffer (Hank's balanced salt solution with

20 mM 4-(2-hydroxyethyl)-1-piperazineethanesulfonic acid, pH 7.4). The transport study was initiated by

incubation of the cells with incubation buffer containing each test compound at 37°C in triplicate. At the

completion of the incubation, cells were quickly washed three times with ice-cold buffer. The cells were

then lysed with methanol containing the internal standard for LC-MS/MS quantification (Supplemental

Methods). The uptake of compounds was normalized by total cell protein using the BCA Protein Assay Kit

following the manufacturer's protocol.

Time Dependent Inhibition (TDI) Study in Human Liver Microsomes (HLM) and Human

Hepatocytes. TDI of CYP3A in HLM was measured in pooled HLM (0.3 mg/mL) in the presence of MgCl₂

(3.3 mM) and NADPH (1.3 mM) in potassium phosphate buffer (100 mM, pH 7.4). TVR stock solutions,

prepared at 100-times the incubation concentration in 90% acetonitrile and 10% water, were added to

this incubation mixture to initiate the reaction. Final incubation concentration range was 0.03-30 µM. At

various time points (1, 2, 4, 9, 14, 21, and 30 min) an aliquot of this mixture was transferred to an activity

incubation mixture consisting of midazolam (20.9 µM, which is approximately 10-fold K_m in HLM), MgCl$_2$

(3.3 mM), and NADPH (1.3 mM) in potassium phosphate buffer (100 mM, pH 7.4), resulting in a 20-fold

dilution. TDI of CYP3A in human hepatocytes was measured in pooled human hepatocytes (0.45 × 10^6

cells/mL) suspended in William's medium E supplemented with L-glutamine and HEPES. TVR stock

solutions, prepared at 10-times the incubation concentration in 90% media, 9% acetonitrile and 1% water,

were added to this incubation mixture to initiate the reaction. Final incubation concentration range was

0.1-30 µM in a volume of 50 µL. At various time points (1, 8, 18, 30, 60, and 90 min), a 200 µL aliquot of

activity incubation mixture consisting of midazolam (final concentration 80 µM, which is approximately 5-

fold K_m in human hepatocytes) in media was added to incubation wells, resulting in a 5-fold dilution. All

reactions were conducted in duplicate at 37 °C with a final volume of 200 µL (HLM) or 250 µL

(hepatocytes). After incubation (6 min for HLM and 20 min for human hepatocytes), the activity reaction

was terminated by the addition of two volumes of acetonitrile containing internal standard (100 ng/mL of

D4-1'-hydroxymidazolam). Samples were vortexed and centrifuged for 5 min at approximately 2300 × g

at room temperature. Supernatant was mixed with an equal volume of water containing 0.2% formic acid

and analyzed directly by LC-MS/MS (Supplemental Methods). For estimation of Kinetic Constants, data

analysis methods have been previously described (Yates et al., 2012).

PBPK Modeling and Simulations. Whole-body PBPK modeling and simulations were performed

using the population-based absorption, distribution, metabolism, and excretion simulator, Simcyp

(version 15, Certara, Sheffield, UK). Each simulation was performed for 50 subjects (5 trials × 10 subjects)

in the software's built-in healthy volunteer virtual population. Dose, dosing interval, and dosing duration

of substrate and perpetrator drugs were similar to that used in the reported clinical studies.

MVC PBPK Model Development. Physicochemical and pharmacokinetic parameters of MVC used

for the present PBPK model are summarized in Table 1. Advanced Dissolution, Absorption, and

Metabolism (ADAM) model and permeability-limited liver distribution model were used to parameterize

drug absorption and liver disposition, respectively. The effective permeability in human ($P_{eff,man}$) was

predicted using apparent permeability (P_{app}) in Caco-2 system (calibrated by propranolol as permeability

marker - 23×10^{-6} cm/s, in house data) (Walker et al., 2005). Colonic absorption of MVC was assumed to

be negligible (regional permeability of colon in ADMA model = 0.01×10^{-4} cm/s). The full-PBPK model was

adopted to obtain the distribution of MVC into all organs except liver using Rodger et al. method

considering rapid equilibrium between blood and tissues with tissue-to-plasma partitioning coefficients

(Kp) (Rodgers et al., 2005; Rodgers and Rowland, 2006). The observed mean pharmacokinetic data of MVC

in healthy subjects receiving 3, 10 and 30 mg MVC via intravenous infusion or 150 mg oral dose were used

to refine absorption and distribution parameters (Abel et al., 2008c; Vourvahis et al., 2014). The Kp scalar

of 1.7 was needed to recover in $vivo$ observed plasma concentration-time profiles. Permeability-limiting

disposition was considered for liver. Intrinsic active uptake clearance and passive diffusion across the

sinusoidal membrane and intrinsic efflux clearance on the canalicular membrane, obtained from SCHH

studies, are used to capture hepatobiliary disposition. The active hepatic uptake clearance was attributed

to OATP1B1-mediated transport based on our data presented (see Results section). On the other hand, P-

gp was assumed to impact on MVC absorption/canalicular efflux (Walker et al., 2005). Intrinsic metabolic

clearance of MVC was obtained using substrate-depletion in HLM incubations (Tseng et al., 2018). The

model with these initial input parameters (transport-metabolism interplay) resulted in underprediction of

hepatic clearance. Therefore, an empirical scaling factor for the hepatic sinusoidal active uptake (SF_{active})

of 10 - estimated by top-down model fitting of the intravenous data - was applied. This SF_{active} is in line

with our previous value reported (Varma et al., 2014). To simulate the effect of inhibitors and inducers on

the MVC pharmacokinetic profile, the models for ketoconazole, efavirenz, rifampicin and ritonavir were

adopted directly from default compound library with certain modifications. P-gp inhibition constant (K_i) of 0.4 μM was added to ketoconazole model. The $K_{i,P\text{-}gp}$ value for ritonavir was also modified to 0.4 μM, instead of a default value of 0.03 μM, which are much below the reported $IC_{50,P\text{-}gp}$ range from 1.5 to 28 μM in Caco-2 cells (Gnoth et al., 2011; Kishimoto et al., 2014). In terms of P-gp induction in gut, rifampicin was assumed to increase intestinal P-gp abundances. Intestinal P-gp expression levels were shown to increase by about 3.5-fold following multiple-dose rifampin treatment, which is similar to the increase in intestinal CYP3A4 level as 4.4-fold (Greiner et al., 1999). Therefore, intestinal P-gp J_{max} of MVC was assumed to be 3.5-fold higher when simulating multiple-dose rifampicin interactions. The $K_{i,OATP1B1}$, CYP3A4 E_{max} and CYP3A4 EC_{50} values of rifampicin were obtained from the previous report to consider impact of rifampicin on CYP3A4 (both inhibition and induction) as well as inhibition of OATP1B1 at concomitant dose with MVC and rifampicin (Varma et al., 2013).

TVR and VRT-127394 PBPK Model Development. Physicochemical and pharmacokinetic parameters of TVR and its *R*-diastereomer VRT-127394 (M0) used for the present PBPK model are summarized in Table 1. The observed mean pharmacokinetic data of TVR and M0 in healthy subjects receiving 750 mg oral single and multiple dose were used to refine input parameters in Absorption, Distribution and Elimination (INCIVEK (telaprevir)). The absorption of TVR was described with the first-order model and distribution was described using the minimal PBPK distribution model. The formation of M0 was assumed as a result of TVR metabolism generated by non CYP3A pathway. The distribution of M0 was described with a minimal PBPK model, and the clearance was assumed to be driven by further metabolism. The following interaction parameters of TVR were used; $K_{i,CYP3A}$ for testosterone (18.6 μM), $K_{I,CYP3A}$ and $k_{inact,CYP3A}$ in hepatocytes (see Results section), $K_{i,P\text{-}gp}$ (0.48 μM), and $K_{i,OATP1B1}$ (0.11 μM). To verify TVR model and determine *in vivo* K_i values based on clinical DDI data, default compound files of midazolam and digoxin were used as is; and the atorvastatin PBPK model was adopted from a published report (Zhang, 2015). Performance of PBPK model predictions was evaluated by the ratio of predicted and observed

values, and presented as $R_{pred/obs}$. A $R_{pred/obs}$ value between 0.8 and 1.25 was used to assess model

performance.

RESULTS

***In Vitro* Transport of MVC.** The time-course profiles of MVC uptake in SCHH and suspended hepatocytes are shown in Figure 1. MVC showed temperature-dependent uptake in both systems with ~95% reduction in uptake at 4°C compared with 37°C implying active transport. In contrast, 30 and 100 µM rifamycin SV enhanced MVC accumulation in SCHH. Significant biliary excretion was noted in SCHH when incubated with and without Ca^{2+}/Mg^{2+}. Overall, the results of *in vitro* studies employing SCHH suggested active uptake and biliary excretion of MVC. Additionally, temperature-dependent transport was also noted in suspended human hepatocytes. In the uptake studies using transporter-transfected HEK293 cells, MVC was transported by OATP1B1, but not by OATP1B3 and OATP2B1 (Table 2). Moreover, OATP1B1-specific uptake displayed concentration-dependency with a biphasic saturation profile (Figure 2A). Within the concentration range of 2.0 to 31.2 µM, MVC transport conformed to Michaelis-Menten kinetics and was characterized with a K_m of 5 µM and V_{max} of 6.25 pmol/min/mg (Figure 2B). The former is lower than the K_m (34 µM) reported using OATP1B1 transfected oocytes (Siccardi et al., 2010). Similar to the stimulatory effect of rifamycin SV noted in SCHH, OATP1B1-mediated uptake of MVC also increased with 100 µM rifamycin SV in transfected HEK293 cells. On the other hand, MVC uptake was inhibited by 100 µM TVR (Figure 2C).

***In Vitro* CYP3A TDI of TVR.** TDI kinetic parameters of TVR for CYP3A were determined with HLM and human hepatocytes using midazolam as a CYP3A probe substrate (Figure 3 and Supplemental Figure 1). Estimated K_I and k_{inact} in HLM were 0.644 µM and 0.108 min^{-1}, respectively. Those values are close to those previously reported by the two independent studies: 1.5 µM and 0.065 min^{-1}; 0.511 µM and 0.113 min^{-1}, respectively (INCIVEK (telaprevir); Oda and Yamano, 2014). The TDI kinetic parameters obtained with human hepatocytes were determined to be K_I of 2.24 µM and k_{inact} of 0.0112 min^{-1}. Thus, the K_I value in human hepatocytes is approximately 3.5-fold higher versus HLM, whereas the k_{inact} in human

hepatocytes is approximately 10-fold lower than that obtained with HLM, resulting in the 33.6-fold difference in the inactivation efficiency (k_{inact}/K_I) between the two systems. The K_I and k_{inact} values obtained with human hepatocytes were used for DDI prediction and were compared to predictions based on HLM-derived parameters.

PBPK Modeling and Simulations of MVC. A PBPK model for MVC, incorporating transporter function for P-gp and OATP1B1, was developed. The simulated MVC plasma concentration-time profiles and pharmacokinetic parameters were in good agreement with the observed clinical data (Table 3 and Supplemental Figure 2A). Also, the predicted MVC bioavailability (F) – estimated based on simulated AUC_{inf} following an intravenous (30 mg) and oral (100 mg) dose – of ~17% agreed with the clinical observation of ~23% at the same oral dose. Fraction of the dose absorbed from gastrointestinal tract (Fa) × fraction of the dose that escapes intestinal first-pass metabolism (Fg) was calculated to be 0.44, which is an underprediction with the observed Fa×Fg of 0.71 estimated from the clinical pharmacokinetics. This difference might be due to notable variability in pharmacokinetics across studies. The MVC model predicted fraction of dose eliminated via renal and hepatic as 0.3 and 0.7, respectively, which are in line with clinical mass balance study (0.25 of renal and 0.75 of hepatic) (Abel et al., 2008c). The model was further used to quantitatively evaluate the observed clinical DDI between MVC and inhibitors/inducers.

Determination of K_i of TVR for Transporters. A PBPK model for TVR including its *R*-diastereomer, M0, was developed using physicochemical and *in vitro* parameters. The simulated TVR plasma concentration-time profiles and pharmacokinetic parameters are in good agreement with the observed clinical data (Table 3 and Supplemental Figure 2B). The *in vivo* K_i values for CYP3A, P-gp and OATP1B1 were determined based on clinical DDI data obtained with the corresponding probe substrates midazolam (CYP3A), digoxin (P-gp) and atorvastatin (CYP3A and OATP1B1). The predicted AUC ratios (AUCRs) of these substrates are summarized in Table 4. HLM-derived TDI parameters for TVR over-predicted (3.4- to 3.7-

fold) the AUCRs of midazolam compared with the clinically observed AUCR. In contrast, human

hepatocyte-based TDI parameters rendered improved predictions of midazolam AUCR (i.e., $R_{pred/obs}$ of 1.1

to 1.3), which model performance was within a range, except for atorvastatin-TVR DDI. *In vivo* K_i values

for P-gp and OATP1B1 inhibition needed to recover the TVR interactions with digoxin and atorvastatin

were about 10-fold lower than the reported IC_{50} values (4.8 and 1.1 µM, respectively) obtained *in vitro*

(Kunze et al., 2012; Fujita et al., 2013). The same *in vivo* K_i values for P-gp and OATP1B1 were assumed for

M0.

DDI Prediction of MVC. Predicted MVC plasma exposure changes (AUC) in the presence of several

inhibitors or inducers are summarized in Table 5. Increase in MVC exposure with TVR can be well

recovered by considering CYP3A and transporter (P-gp and OATP1B1) inhibition using the *in vivo* K_i values

for TVR (Figure 4A). Based on the sensitivity analysis, use of *in vitro* K_i values for P-gp and OATP1B1

resulted in a predicted AUCR of ~5, however, the optimized K_i values (estimated via PBPK modeling of

probe substrates) recovered MVC AUCR well (Supplemental Figure 3).

Further sensitivity analysis of the MVC-TVR interaction (AUCR and $C_{max}R$) indicated that inhibition of P-gp,

CYP3A or OATP1B1 alone results in about 2-fold increase, and inhibition of CYP3A and either transporter

results in a ~4- to 5-fold increase, while inhibition of all three mechanisms (P-gp, CYP3A, and OATP1B1)

yields about 8-fold increase in AUCR (Figures 4B and 4C). Ketoconazole, a CYP3A inhibitor, and ritonavir,

a CYP3A inhibitor and inducer, were predicted to cause an increase in MVC exposure when incorporating

P-gp inhibition, while efavirenz and rifampicin, which are inducers of CYP3A, were predicted to reduce

MVC AUCR. When MVC DDIs were predicted by using default models of ketoconazole and ritonavir, which

meant $K_{i,P-gp}$ of ketoconazole was not included and that of ritonavir was 0.03, AUCR with ketoconazole was

under-predicted and that with ritonavir was over-predicted ($R_{pred/obs}$ of 0.53 and 1.6, respectively). The

reported P-gp IC_{50} range of ketoconazole and ritonavir using Caco-2 cells was approximately 0.24 to 3.4

and 1.5 to 28 μM, respectively (Gnoth et al., 2011; Kishimoto et al., 2014; Mikkaichi et al., 2014). Therefore, the prediction of AUCR using $K_{i,P-gp}$ of ketoconazole and ritonavir set at 0.4 μM, improved $R_{pred/obs}$ to 0.81 and 1.1, respectively. The MVC DDI with rifampicin was also predicted using a PBPK model assuming increased intestinal P-gp J_{max} (i.e., 4-fold increase corresponding to P-gp expression change in intestine on rifampicin treatment) and OATP1B1 inhibition. Accounting for intestinal P-gp induction along with hepatic OATP1B1 inhibition resulted in a predicted AUCR of 0.37, which is in line with observed AUCR of 0.33.

DISCUSSION

Our findings from *in vitro* mechanistic studies along with the comprehensive PBPK modeling and simulations, verified with a range of clinical DDI data, provide evidence for the involvement of CYP3A, P-gp and OATP1B1 in determining the pharmacokinetics and drug interactions of MVC (Figure 5).

We characterized the hepatic transporter-mediated disposition of MVC using transfected HEK293 cells and cryopreserved human primary hepatocytes. The present study provided additional *in vitro* data in support of OATP substrate activity. First, uptake by OATP1B1-transfected (versus mock-transfected HEK293) cells was evident (uptake ratio of ~3), which conformed to two-K_m kinetics (Table 2, Figure 2A). Second, temperature-dependent uptake of MVC was observed in human hepatocyte systems (Figures 1A and 1B). However, unexpectedly, 100 μM rifamycin SV (a pan-OATP inhibitor) stimulated MVC uptake in both OATP1B1-transfected cells and SCHH (Figures 1A, 1C and 2C). Stimulation of uptake for several OATP substrates in the presence of inhibitors is well documented, and may involve mechanisms such as cis- and/or trans-stimulation and allosterism (Wang et al., 2005; Kimoto et al., 2011; Roth et al., 2011; Wlcek et al., 2013; Varma et al., 2016). Since this phenomenon was observed in both transfected cells and human hepatocytes, potential inhibition of metabolism or basolateral efflux transporters by rifamycin SV can be ruled out. Nevertheless, our studies with transfected cells indicated inhibition of MVC uptake by TVR (Figure 2C), which has been previously shown to be an OATP inhibitor (Kunze et al., 2012; Chu et al., 2013; Furihata et al., 2014). It is therefore important to consider other experimental conditions (e.g., additional OATP inhibitors and incubation at 4°C) in the process of evaluating the role for hepatic uptake in the clearance of drugs, particularly when stimulation of activity is noted *in vitro*.

Although the high resolution structure of OATP1B1 has not been solved, numerous groups have reported that substrates such as estrone-3-sulfate present multiphasic uptake kinetics plausibly due to more than one substrate binding site (Tamai et al., 2001; Noe et al., 2007; Gui and Hagenbuch, 2009).

Further evidence for the presence of multiple binding sites comes from the observed stimulation of transport of some substrates by known OATP inhibitors (Wang et al., 2005; Wlcek et al., 2013). Earlier studies using cysteine scanning mutagenesis suggested that a set of common but not identical amino acids on a transmembrane domain 10 of OATP1B1 are involved in the substrate binding sites/translocation pathways for the different substrates; and that certain translocation pathways are stimulated while others are inhibited by the same inhibitor (Ohnishi et al., 2014). Our *in vitro* studies showed that, (i) the uptake of MVC was biphasic in the OATP1B1-expressed HEK293 cells, and (ii) notable stimulation of MVC uptake by rifamycin SV (Figures 1A, 1C and 2C) and cyclosporin A (data not shown, 160% of control) but inhibition by TVR (Figure 2C). Taken together, our results suggest different binding sites on OATP1B1 and that possibly MVC and TVR are competing for the same binding pocket.

The DDI predictions for CYP3A probe substrate (intravenous and oral midazolam) using TVR TDI parameters obtained from human hepatocytes were in good agreement with the observed data, while those estimated using HLM considerably over-predicted (Table 4). Consistent with our results, certain CYP3A inhibitors were also presented with higher inactivation potency in HLM, and the TDI parameters obtained using human hepatocytes better recovered clinical DDIs (Xu et al., 2009; Chen et al., 2011; Mao et al., 2013; Mao et al., 2016). System-dependent apparent differences in K_I may be attributed to the lower intracellular concentrations of the inhibitor at the site of the enzyme (hepatocytes versus HLM). It should be noted that many of these drugs including TVR are P-gp substrates *in vitro* and could be subjected to efflux in hepatocytes (INCIVEK (telaprevir); White et al., 2010; Weiss et al., 2014). On the other hand, lower k_{inact} in human hepatocytes may be driven by the differences in enzyme expression, sequential metabolism including intermediate complexes or the concentration of inhibitor and/or metabolite(s) in cells. The estimated inactivation parameters (k_{inact} and K_I) in human hepatocytes can be considered as an apparent hybrid parameter between the rate of diffusion through the cell membrane, the total metabolic consumption rate (including sequential metabolism), and the intrinsic enzyme inactivation rate. Further

mechanistic studies are warranted to understand the notable differences between human hepatocytes and HLM. Nevertheless, the current study suggests that human hepatocytes, which are physiologically relevant and closer to *in vivo*, should be considered when prospectively modeling DDI involving TDI of CYP3A.

A full PBPK model was developed for MVC, assuming permeability-limited hepatic disposition (OATP1B1-CYP3A interplay) to quantitatively rationalize clinical DDIs of MVC as a victim drug (Figure 5). TVR PBPK model including its *R*-diastereomer, M0, was also developed, wherein transporter- and enzyme-based interactions are captured. Hepatocyte-to-plasma unbound ratio of TVR and M0 was assumed to be 1 in the model. M0 (also referred as VRT-127394) was found to be at equivalent levels to TVR in plasma at steady-state (INCIVEK (telaprevir)). We therefore developed a model for the metabolite and assumed that the inhibitory potency of M0 against P-gp and OATP1B1 is similar to TVR. Inhibition potency of TVR including M0 in the model was refined and verified based on its clinical interactions with probe substrates: midazolam for CYP3A, digoxin for P-gp, and atorvastatin for CYP3A, OATP1B1 and P-gp. Collectively, the modeling and simulations suggested that TVR clinical DDIs with probe substrates for CYP3A, P-gp and OATP1B1 are well described when considering (i) *in vitro* CYP3A reversible inhibition of TVR and M0, (ii) *in vitro* K_I and k_{inact} of TVR obtained from human hepatocytes, and (iii) P-gp and OATP1B1 reversible inhibition by TVR and M0 with ~10-fold lower (optimized) K_i than noted in the *in vitro* inhibition values. Previous studies from our group and others have highlighted the need for transporter K_i values to be lower than those observed *in vitro* to recover clinical DDIs (Varma et al., 2012; Yoshikado et al., 2016; Shebley et al., 2017; Barnett et al., 2018). The empirical correction of *in vitro* transporter K_i may add some degree of uncertainty to the interpretation of quantitative contribution of the individual mechanisms to the noted DDIs. The potential TDI for transporters, such as cyclosporin A, could be one possibility (Takahashi et al., 2016; Shitara and Sugiyama, 2017). Nevertheless, our cross-validation approach to verify individual interaction mechanisms of TVR using clinical data from probe substrates (e.g., midazolam for CYP3A,

digoxin for P-gp and atorvastatin for OATP1B1) provided rationale for such empirical corrections to the less understood *in vitro-in vivo* disconnect in transporter inhibition potency.

Ketoconazole is often used as a CYP3A probe inhibitor in clinical DDI studies, however, it can inhibit intestinal P-gp (IC_{50} range of 0.42 to 3.4 μM) (Kishimoto et al., 2014; Mikkaichi et al., 2014). In this regard, clinical studies have demonstrated a significant increase in plasma exposure of metabolically stable drugs such as fexofenadine (P-gp substrate) by ketoconazole (ALLEGRA® (fexofenadine hydrochloride)). Moreover, no change was observed in monkeys after intravenous administration of fexofenadine with ketoconazole, while its oral bioavailability increased approximately 2-fold (Ogasawara et al., 2007). Similarly, ritonavir inhibits CYP3A along with P-gp. Clinical evidence implies increase in plasma exposure of digoxin by ritonavir due to P-gp inhibition (Penzak et al., 2004; Kirby et al., 2012). In line with these observations, PBPK modeling of ketoconazole and ritonavir interactions with probe substrates and MVC using *in vivo* $K_{i,P-gp}$ of 0.4 μM, supported the role of P-gp in limiting the intestinal absorption of MVC. Consequently, inhibition of intestinal P-gp likely contributes to the observed strong interaction between MVC and TVR.

Rifampicin induces not only CYP3A but also P-gp at the intestine (Chen and Raymond, 2006). Greiner et al. reported that oral exposure of digoxin is reduced by about 2-fold with multi-dose rifampicin treatment, although intravenous exposure of digoxin is less affected (Greiner et al., 1999). The same study also showed about 4-fold increase in intestinal P-gp expression levels in the rifampicin-treatment group, suggesting that increased efflux further limited digoxin absorption. Since MVC is a dual-substrate for CYP3A and P-gp, the decrease in MVC exposure by rifampicin could be explained by induction of both CYP3A and P-gp in the gut. In addition, a model-based analysis has suggested that a concomitant dose of rifampicin following chronic treatment impose dual effects of CYP3A induction and OATP1B1 inhibition (Varma et al., 2013). Consistently, PBPK simulations of MVC-rifampicin DDI were in good agreement with

the observed data when assuming a 4-fold induction of intestinal P-gp and simultaneous inhibition of OATP1B1-mediated hepatic uptake in addition to the CYP3A induction. Efavirenz (a moderate CYP3A inducer) does not induce intestinal P-gp expression in humans (Mouly et al., 2002; Oswald et al., 2012), and is not an OATP1B1 inhibitor at clinically relevant concentrations (Karlgren et al., 2012). Therefore, the MVC-efavirenz interaction could be well described by considering CYP3A induction only. The prediction results of MVC DDI with ketoconazole, ritonavir, efavirenz and rifampicin suggested that MVC oral clearance is determined by not only CYP3A4-mediated metabolism, but also P-gp-mediated intestinal efflux. Overall, this study emphasizes the need to capture intestinal P-gp when rationalizing or prospectively predicting interactions with perpetrator drugs like ketoconazole (CYP3A inhibitor) and rifampicin (CYP3A inducer).

In summary, our *in vitro* mechanistic studies and PBPK modeling and simulations suggest that (i) OATP1B1-mediated uptake along with CYP3A determine the hepatic clearance of MVC, and thus contribute to the interaction with TVR, (ii) CYP3A inactivation parameters of TVR from human hepatocytes well predict the clinical interactions with probe substrates, and (iii) P-gp-mediated intestinal efflux limits the intestinal absorption of MVC, and drugs like TVR, ketoconazole and rifampicin effect its oral exposure by modulating the P-gp function/expression. Finally, this study presents a comprehensive case example for quantitative de-convolution of multiple mechanisms including complex scenarios, such as transporter-enzyme interplay, metabolite contribution and combined intestinal-liver disposition often involved in clinical DDIs.

ACKNOWLEDGMENTS

AUTHORSHIP CONTRIBUTIONS

Participated in research design: EK, MV, MVSV

Conducted experiments: EK, RJS, HE

Performed data analysis: EK

Wrote or contributed to the writing of the manuscript: EK, MV, RJS, HE, ADR, MVSV

REFERENCES

Abel S, Back DJ, and Vourvahis M (2009) Maraviroc: pharmacokinetics and drug interactions. *Antiviral therapy* **14:**607-618.

Abel S, Jenkins TM, Whitlock LA, Ridgway CE, and Muirhead GJ (2008a) Effects of CYP3A4 inducers with and without CYP3A4 inhibitors on the pharmacokinetics of maraviroc in healthy volunteers. *British journal of clinical pharmacology* **65 Suppl 1:**38-46.

Abel S, Russell D, Taylor-Worth RJ, Ridgway CE, and Muirhead GJ (2008b) Effects of CYP3A4 inhibitors on the pharmacokinetics of maraviroc in healthy volunteers. *British journal of clinical pharmacology* **65 Suppl 1:**27-37.

Abel S, Russell D, Whitlock LA, Ridgway CE, Nedderman AN, and Walker DK (2008c) Assessment of the absorption, metabolism and absolute bioavailability of maraviroc in healthy male subjects. *British journal of clinical pharmacology* **65 Suppl 1:**60-67.

ALLEGRA® (fexofenadine hydrochloride) Sanofi S.A. Package Insert. *US Department of Health and Human Services, US Food and Drug Administration, Rockville, MD* https://www.accessdata.fda.gov/drugsatfda_docs/label/2003/20786se20788-20014,20872se20788-20011,20625se20788-20012_allegra_lbl.pdf.

Barnett S, Ogungbenro K, Menochet K, Shen H, Lai Y, Humphreys WG, and Galetin A (2018) Gaining Mechanistic Insight Into Coproporphyrin I as Endogenous Biomarker for OATP1B-Mediated Drug-Drug Interactions Using Population Pharmacokinetic Modeling and Simulation. *Clinical pharmacology and therapeutics* **104:**564-574.

Bi YA, Qiu X, Rotter CJ, Kimoto E, Piotrowski M, Varma MV, Ei-Kattan AF, and Lai Y (2013) Quantitative assessment of the contribution of sodium-dependent taurocholate co-transporting polypeptide (NTCP) to the hepatic uptake of rosuvastatin, pitavastatin and fluvastatin. *Biopharmaceutics & drug disposition* **34:**452-461.

Center for Drug Evaluation and Research (CDER) (2017) Guidance for Industry: Drug Interaction Studies– Study Design, Data Analysis, Implications for Dosing, and Labeling Recommendations [Draft Guidance]. *US Department of Health and Human Services, US Food and Drug Administration, Rockville, MD* http://www.fda.gov/downloads/Drugs/Guidance-ComplianceRegulatoryInformation/Guidances/ucm292362.pdf.

Chen J and Raymond K (2006) Roles of rifampicin in drug-drug interactions: underlying molecular mechanisms involving the nuclear pregnane X receptor. *Annals of clinical microbiology and antimicrobials* **5:**3.

Chen Y, Liu L, Monshouwer M, and Fretland AJ (2011) Determination of time-dependent inactivation of CYP3A4 in cryopreserved human hepatocytes and assessment of human drug-drug interactions. *Drug metabolism and disposition: the biological fate of chemicals* **39:**2085-2092.

Chu X, Cai X, Cui D, Tang C, Ghosal A, Chan G, Green MD, Kuo Y, Liang Y, Maciolek CM, Palamanda J, Evers R, and Prueksaritanont T (2013) In vitro assessment of drug-drug interaction potential of boceprevir associated with drug metabolizing enzymes and transporters. *Drug metabolism and disposition: the biological fate of chemicals* **41:**668-681.

Committee for Human Medicinal Products (CHMP) (2012) Guideline on the Investigation of Drug Interactions [Final]. *European Medicines Agency, London* http://www.ema.europa.eu/docs/en_GB/document_library/Scientific_guideline/2012/2007/WC500129606.pdf.

Fahmi OA, Hurst S, Plowchalk D, Cook J, Guo F, Youdim K, Dickins M, Phipps A, Darekar A, Hyland R, and Obach RS (2009) Comparison of different algorithms for predicting clinical drug-drug interactions, based on the use of CYP3A4 in vitro data: predictions of compounds as precipitants of interaction. *Drug metabolism and disposition: the biological fate of chemicals* **37:**1658-1666.

Fujita Y, Noguchi K, Suzuki T, Katayama K, and Sugimoto Y (2013) Biochemical interaction of anti-HCV telaprevir with the ABC transporters P-glycoprotein and breast cancer resistance protein. *BMC research notes* **6:**445.

Furihata T, Matsumoto S, Fu Z, Tsubota A, Sun Y, Matsumoto S, Kobayashi K, and Chiba K (2014) Different interaction profiles of direct-acting anti-hepatitis C virus agents with human organic anion transporting polypeptides. *Antimicrobial agents and chemotherapy* **58:**4555-4564.

Gnoth MJ, Buetehorn U, Muenster U, Schwarz T, and Sandmann S (2011) In vitro and in vivo P-glycoprotein transport characteristics of rivaroxaban. *The Journal of pharmacology and experimental therapeutics* **338:**372-380.

Greiner B, Eichelbaum M, Fritz P, Kreichgauer HP, von Richter O, Zundler J, and Kroemer HK (1999) The role of intestinal P-glycoprotein in the interaction of digoxin and rifampin. *The Journal of clinical investigation* **104:**147-153.

Gui C and Hagenbuch B (2009) Role of transmembrane domain 10 for the function of organic anion transporting polypeptide 1B1. *Protein science : a publication of the Protein Society* **18:**2298-2306.

Hyland R, Dickins M, Collins C, Jones H, and Jones B (2008) Maraviroc: in vitro assessment of drug-drug interaction potential. *British journal of clinical pharmacology* **66:**498-507.

INCIVEK (telaprevir) Vertex Pharmaceuticals Inc. Clinical Pharmacology Biopharmaceutics Review(s). *FDA Access File, US Food and Drug Administration* https://www.accessdata.fda.gov/drugsatfda_docs/nda/2011/201917Orig201911s201000ClinPharmR.pdf

Karlgren M, Vildhede A, Norinder U, Wisniewski JR, Kimoto E, Lai Y, Haglund U, and Artursson P (2012) Classification of inhibitors of hepatic organic anion transporting polypeptides (OATPs): influence of protein expression on drug-drug interactions. *Journal of medicinal chemistry* **55:**4740-4763.

Kimoto E, Bi YA, Kosa RE, Tremaine LM, and Varma MVS (2017) Hepatobiliary Clearance Prediction: Species Scaling From Monkey, Dog, and Rat, and In Vitro-In Vivo Extrapolation of Sandwich-Cultured Human Hepatocytes Using 17 Drugs. *Journal of pharmaceutical sciences* **106:**2795-2804.

Kimoto E, Chupka J, Xiao Y, Bi YA, and Duignan DB (2011) Characterization of digoxin uptake in sandwich-cultured human hepatocytes. *Drug metabolism and disposition: the biological fate of chemicals* **39:**47-53.

Kimoto E, Li R, Scialis RJ, Lai Y, and Varma MV (2015) Hepatic Disposition of Gemfibrozil and Its Major Metabolite Gemfibrozil 1-O-beta-Glucuronide. *Molecular pharmaceutics* **12:**3943-3952.

Kirby BJ, Collier AC, Kharasch ED, Whittington D, Thummel KE, and Unadkat JD (2012) Complex drug interactions of the HIV protease inhibitors 3: effect of simultaneous or staggered dosing of digoxin and ritonavir, nelfinavir, rifampin, or bupropion. *Drug metabolism and disposition: the biological fate of chemicals* **40:**610-616.

Kishimoto W, Ishiguro N, Ludwig-Schwellinger E, Ebner T, and Schaefer O (2014) In vitro predictability of drug-drug interaction likelihood of P-glycoprotein-mediated efflux of dabigatran etexilate based on [I]2/IC50 threshold. *Drug metabolism and disposition: the biological fate of chemicals* **42:**257-263.

Kunze A, Huwyler J, Camenisch G, and Gutmann H (2012) Interaction of the antiviral drug telaprevir with renal and hepatic drug transporters. *Biochemical pharmacology* **84:**1096-1102.

Mao J, Johnson TR, Shen Z, and Yamazaki S (2013) Prediction of crizotinib-midazolam interaction using the Simcyp population-based simulator: comparison of CYP3A time-dependent inhibition between human liver microsomes versus hepatocytes. *Drug metabolism and disposition: the biological fate of chemicals* **41:**343-352.

Mao J, Tay S, Khojasteh CS, Chen Y, Hop CE, and Kenny JR (2016) Evaluation of Time Dependent Inhibition Assays for Marketed Oncology Drugs: Comparison of Human Hepatocytes and Liver Microsomes in the Presence and Absence of Human Plasma. *Pharmaceutical research* **33:**1204-1219.

Mikkaichi T, Yoshigae Y, Masumoto H, Imaoka T, Rozehnal V, Fischer T, Okudaira N, and Izumi T (2014) Edoxaban transport via P-glycoprotein is a key factor for the drug's disposition. *Drug metabolism and disposition: the biological fate of chemicals* **42:**520-528.

Mouly S, Lown KS, Kornhauser D, Joseph JL, Fiske WD, Benedek IH, and Watkins PB (2002) Hepatic but not intestinal CYP3A4 displays dose-dependent induction by efavirenz in humans. *Clinical pharmacology and therapeutics* **72:**1-9.

Noe J, Portmann R, Brun ME, and Funk C (2007) Substrate-dependent drug-drug interactions between gemfibrozil, fluvastatin and other organic anion-transporting peptide (OATP) substrates on OATP1B1, OATP2B1, and OATP1B3. *Drug metabolism and disposition: the biological fate of chemicals* **35:**1308-1314.

Oda K and Yamano K (2014) Effect of telaprevir on the metabolism and hepatic uptake of tacrolimus (FK506). *Biopharmaceutics & drug disposition* **35:**501-512.

Ogasawara A, Kume T, and Kazama E (2007) Effect of oral ketoconazole on intestinal first-pass effect of midazolam and fexofenadine in cynomolgus monkeys. *Drug metabolism and disposition: the biological fate of chemicals* **35:**410-418.

Ohnishi S, Hays A, and Hagenbuch B (2014) Cysteine scanning mutagenesis of transmembrane domain 10 in organic anion transporting polypeptide 1B1. *Biochemistry* **53:**2261-2270.

Oswald S, Meyer zu Schwabedissen HE, Nassif A, Modess C, Desta Z, Ogburn ET, Mostertz J, Keiser M, Jia J, Hubeny A, Ulrich A, Runge D, Marinova M, Lutjohann D, Kroemer HK, and Siegmund W (2012) Impact of efavirenz on intestinal metabolism and transport: insights from an interaction study with ezetimibe in healthy volunteers. *Clinical pharmacology and therapeutics* **91:**506-513.

Penzak SR, Shen JM, Alfaro RM, Remaley AT, Natarajan V, and Falloon J (2004) Ritonavir decreases the nonrenal clearance of digoxin in healthy volunteers with known MDR1 genotypes. *Therapeutic drug monitoring* **26:**322-330.

Platt L, Easterbrook P, Gower E, McDonald B, Sabin K, McGowan C, Yanny I, Razavi H, and Vickerman P (2016) Prevalence and burden of HCV co-infection in people living with HIV: a global systematic review and meta-analysis. *The Lancet Infectious diseases* **16:**797-808.

Rodgers T, Leahy D, and Rowland M (2005) Physiologically based pharmacokinetic modeling 1: predicting the tissue distribution of moderate-to-strong bases. *Journal of pharmaceutical sciences* **94:**1259-1276.

Rodgers T and Rowland M (2006) Physiologically based pharmacokinetic modelling 2: predicting the tissue distribution of acids, very weak bases, neutrals and zwitterions. *Journal of pharmaceutical sciences* **95:**1238-1257.

Roth M, Timmermann BN, and Hagenbuch B (2011) Interactions of green tea catechins with organic anion-transporting polypeptides. *Drug metabolism and disposition: the biological fate of chemicals* **39:**920-926.

Shebley M, Fu W, Badri P, Bow D, and Fischer V (2017) Physiologically Based Pharmacokinetic Modeling Suggests Limited Drug-Drug Interaction Between Clopidogrel and Dasabuvir. *Clinical pharmacology and therapeutics* **102:**679-687.

Shitara Y and Sugiyama Y (2017) Preincubation-dependent and long-lasting inhibition of organic anion transporting polypeptide (OATP) and its impact on drug-drug interactions. *Pharmacology & therapeutics* **177:**67-80.

Siccardi M, D'Avolio A, Nozza S, Simiele M, Baietto L, Stefani FR, Moss D, Kwan WS, Castagna A, Lazzarin A, Calcagno A, Bonora S, Back D, Di Perri G, and Owen A (2010) Maraviroc is a substrate for OATP1B1 in vitro and maraviroc plasma concentrations are influenced by SLCO1B1 521 T>C polymorphism. *Pharmacogenetics and genomics* **20:**759-765.

Takahashi T, Ohtsuka T, Uno Y, Utoh M, Yamazaki H, and Kume T (2016) Pre-incubation with cyclosporine A potentiates its inhibitory effects on pitavastatin uptake mediated by recombinantly expressed

cynomolgus monkey hepatic organic anion transporting polypeptide. *Biopharmaceutics & drug disposition* **37:**479-490.

Tamai I, Nozawa T, Koshida M, Nezu J, Sai Y, and Tsuji A (2001) Functional characterization of human organic anion transporting polypeptide B (OATP-B) in comparison with liver-specific OATP-C. *Pharmaceutical research* **18:**1262-1269.

The Japanese Ministry of Health L, and Welfare (MHLW) (2014) Drug interaction guideline for drug development and labeling recommendation (draft). *Pharmaceuticals and Medical Devices Agency, Tokyo*:https://www.solvobiotech.com/documents/Japanese_DDI_guideline_(draft)_2014Jan.pdf.

Tseng E, Fate GD, Walker GS, Goosen TC, and Obach RS (2018) Biosynthesis and Identification of Metabolites of Maraviroc and Their Use in Experiments to Delineate the Relative Contributions of Cytochrome P4503A4 versus 3A5. *Drug metabolism and disposition: the biological fate of chemicals* **46:**493-502.

Varma MV, Bi YA, Kimoto E, and Lin J (2014) Quantitative prediction of transporter- and enzyme-mediated clinical drug-drug interactions of organic anion-transporting polypeptide 1B1 substrates using a mechanistic net-effect model. *The Journal of pharmacology and experimental therapeutics* **351:**214-223.

Varma MV, Kimoto E, Scialis R, Bi Y, Lin J, Eng H, Kalgutkar AS, El-Kattan AF, Rodrigues AD, and Tremaine LM (2016) Transporter-Mediated Hepatic Uptake Plays an Important Role in the Pharmacokinetics and Drug-Drug Interactions of Montelukast. *Clinical pharmacology and therapeutics* **101:**406-415.

Varma MV, Lai Y, Feng B, Litchfield J, Goosen TC, and Bergman A (2012) Physiologically based modeling of pravastatin transporter-mediated hepatobiliary disposition and drug-drug interactions. *Pharmaceutical research* **29:**2860-2873.

Varma MV, Lin J, Bi YA, Rotter CJ, Fahmi OA, Lam JL, El-Kattan AF, Goosen TC, and Lai Y (2013) Quantitative prediction of repaglinide-rifampicin complex drug interactions using dynamic and static mechanistic models: delineating differential CYP3A4 induction and OATP1B1 inhibition potential of rifampicin. *Drug metabolism and disposition: the biological fate of chemicals* **41:**966-974.

Varma MV, Pang KS, Isoherranen N, and Zhao P (2015) Dealing with the complex drug-drug interactions: towards mechanistic models. *Biopharmaceutics & drug disposition* **36:**71-92.

Vieira ML, Kirby B, Ragueneau-Majlessi I, Galetin A, Chien JY, Einolf HJ, Fahmi OA, Fischer V, Fretland A, Grime K, Hall SD, Higgs R, Plowchalk D, Riley R, Seibert E, Skordos K, Snoeys J, Venkatakrishnan K, Waterhouse T, Obach RS, Berglund EG, Zhang L, Zhao P, Reynolds KS, and Huang SM (2014) Evaluation of various static in vitro-in vivo extrapolation models for risk assessment of the CYP3A inhibition potential of an investigational drug. *Clinical pharmacology and therapeutics* **95:**189-198.

Vourvahis M, Plotka A, Kantaridis C, Fang A, and Heera J (2014) The effects of boceprevir and telaprevir on the pharmacokinetics of maraviroc: an open-label, fixed-sequence study in healthy volunteers. *Journal of acquired immune deficiency syndromes (1999)* **65:**564-570.

Vourvahis M, Sanders F, Malarstig A, Morgan P, Fenner KS, Wood LS, Lin CY, Ullah M, Kempshall S, Siccardi M, and Owen A (2011) Impact of genetic variants of OATP1B1 (SLCO1B1) on maraviroc pharmacokinetics. *13th European AIDS Conference (EACS), Belgrade, Serbia*.

Wagner C, Zhao P, Pan Y, Hsu V, Grillo J, Huang SM, and Sinha V (2015) Application of Physiologically Based Pharmacokinetic (PBPK) Modeling to Support Dose Selection: Report of an FDA Public Workshop on PBPK. *CPT: pharmacometrics & systems pharmacology* **4:**226-230.

Walker DK, Abel S, Comby P, Muirhead GJ, Nedderman AN, and Smith DA (2005) Species differences in the disposition of the CCR5 antagonist, UK-427,857, a new potential treatment for HIV. *Drug metabolism and disposition: the biological fate of chemicals* **33:**587-595.

Wang X, Wolkoff AW, and Morris ME (2005) Flavonoids as a novel class of human organic anion-transporting polypeptide OATP1B1 (OATP-C) modulators. *Drug metabolism and disposition: the biological fate of chemicals* **33:**1666-1672.

Weiss J, Becker JP, and Haefeli WE (2014) Telaprevir is a substrate and moderate inhibitor of P-glycoprotein, a strong inductor of ABCG2, but not an activator of PXR in vitro. *International journal of antimicrobial agents* **43:**184-188.

White PW, Llinas-Brunet M, Amad M, Bethell RC, Bolger G, Cordingley MG, Duan J, Garneau M, Lagace L, Thibeault D, and Kukolj G (2010) Preclinical characterization of BI 201335, a C-terminal carboxylic acid inhibitor of the hepatitis C virus NS3-NS4A protease. *Antimicrobial agents and chemotherapy* **54:**4611-4618.

Wlcek K, Koller F, Ferenci P, and Stieger B (2013) Hepatocellular organic anion-transporting polypeptides (OATPs) and multidrug resistance-associated protein 2 (MRP2) are inhibited by silibinin. *Drug metabolism and disposition: the biological fate of chemicals* **41:**1522-1528.

Xu L, Chen Y, Pan Y, Skiles GL, and Shou M (2009) Prediction of human drug-drug interactions from time-dependent inactivation of CYP3A4 in primary hepatocytes using a population-based simulator. *Drug metabolism and disposition: the biological fate of chemicals* **37:**2330-2339.

Yates P, Eng H, Di L, and Obach RS (2012) Statistical methods for analysis of time-dependent inhibition of cytochrome p450 enzymes. *Drug metabolism and disposition: the biological fate of chemicals* **40:**2289-2296.

Yoshikado T, Yoshida K, Kotani N, Nakada T, Asaumi R, Toshimoto K, Maeda K, Kusuhara H, and Sugiyama Y (2016) Quantitative Analyses of Hepatic OATP-Mediated Interactions Between Statins and Inhibitors Using PBPK Modeling With a Parameter Optimization Method. *Clinical pharmacology and therapeutics* **100:**513-523.

Zhang T (2015) Physiologically based pharmacokinetic modeling of disposition and drug-drug interactions for atorvastatin and its metabolites. *European journal of pharmaceutical sciences : official journal of the European Federation for Pharmaceutical Sciences* **77:**216-229.

CONFLICT OF INTEREST

The authors have no conflicts of interest that are directly relevant to this study.

LEGENDS FOR FIGURES

Figure 1. Hepatic transport of MVC measured using SCHH and suspended human hepatocytes. The time course of MVC uptake by SCHH (A) and hepatocyte suspension (B) was investigated at 1 µM at 37 °C (●) or 4 °C (□) with standard HBSS in the presence or absence of 100 µM rifamycin SV (△) or with Ca^{2+}/Mg^{2+}-free HBSS (○). Each point represents the mean ± S.D. of 4 to 12 measurements from 1 or 3 studies for A and of triplicate from 1 study for B. Effect of rifamycin SV on MVC uptake (1 µM) in SCHH (C) was investigated at 37 °C for 5 min in the presence or absence of rifamycin SV at 1, 3, 10, 30 and 100 µM. Each point represents the mean ± S.D. (n = 4) from one study.

Figure 2. OATP1B1-mediated uptake of MVC measured in transfected HEK293 cells. Uptake rate was measured at a MVC concentration range of 1.95 to 1000 µM (A) and low K_m was determined in the range of 1.95 to 31 µM (B), at 37 °C. The inset shows an Eadie-Hofstee plot of MVC uptake. The accumulation of MVC (1 µM) was investigated at 37°C in the presence or absence of 100 µM rifamycin SV or 100 µM TVR (C). In C, data points represent the observed data in OATP1B1-HEK without (●) with rifamycin SV (△) or TVR (◇), and wild-type HEK (○). Each point represents the mean ± S.D. (n = 3-6) from one study.

Figure 3. Time-dependent inhibition by TVR for CYP3A in human hepatocytes (A) and HLM (B). Datapoints are the mean of duplicate measurements from one study. The solid line represents the fitting curve to estimate inactivation kinetics – shown in tables (mean ± standard error). Inactivation plots to determine Kobs are in supplemental Figure S1.

Figure 4. A, PBPK model-based prediction of the concentration-time profile of MVC in the presence or absence of TVR. Simulations were based on the dosage regimen used in the clinical study (Vourvahis et al., 2014). Treatment 1, MVC 150 mg b.i.d. for 5 days; Treatment 2, MVC 150 mg b.i.d. plus TVR 750 mg t.i.d. for 10 days was administered. Solid lines and circles represent simulated and observed data, respectively. Blue and pink shaded areas represent 95% CI of MVC simulated plasma concentration when dosed alone or with TVR, respectively. B and C, Predicted effect of TVR on MVC AUCR and $C_{max}R$, assuming P-gp inhibition alone, CYP3A inhibition alone, OATP1B1 inhibition alone, inhibition of both CYP3A and OATP1B1, and inhibition of all mechanisms. Horizontal line with shaded area represents mean and 95% CI of observed AUCR or $C_{max}R$. In plots B and C, circles represent simulated individual values (population size of 50). Lines and error bars denote mean and S.D.

Figure 5. A schematic of MVC disposition and DDI mechanisms is illustrated. MVC is taken up into hepatocytes across the sinusoidal membrane by passive and active uptake via OATP1B1, and is subjected to efflux into bile across the canalicular membrane via P-gp. MVC is primarily metabolized by CYP3A in gut and liver. Intestinal P-gp-mediated efflux influence MVC absorption. Renal clearance of MVC is about 23% of total clearance. MVC, maraviroc; TVR, telaprevir; KET, ketoconazole; RVR, ritonavir; EFV, efavirenz; RIF, rifampicin.

TABLES

Table 1. Summary of Input Parameters for PBPK models of MVC, TVR and M0

Parameters (unit)	MVC		TVR (*S*-configuration)		M0 (*R*-diastereomer)	
	Input value	Source/Comments	Input value	Source/Comments	Input value	Source/Comments
Physicochemical properties						
Molecular weight (g/mol)	513.7	(Hyland et al., 2008)	679.85	(INCIVEK (telaprevir))	679.85	Same as TVR
logP	2.4	(Hyland et al., 2008)	4	(INCIVEK (telaprevir))	4	Same as TVR
Compound type	Monoprotic basic	(Hyland et al., 2008)	Neutral	(INCIVEK (telaprevir))	Neutral	Same as TVR
pKa	7.3	(Hyland et al., 2008)				
Plasma fraction unbound (fu,p)	0.25	(Hyland et al., 2008)	0.41	(INCIVEK (telaprevir))	0.41	Same as TVR
Blood/plasma ratio (Rb)	0.59	(Hyland et al., 2008)	0.65	(INCIVEK (telaprevir))	0.65	Same as TVR
Absorption						
Absorption type	ADAM*		1st order			
Caco-2 permeability ($\times 10^{-6}$ cm/s)	2.7	Measured	-			
Permeability calibrator, Propranolol ($\times 10^{-6}$ cm/s)	23	Measured	-			
First-order absorption arte constant (1/hr)	-		0.8	Optimized according to clinical data		
Lag time (hr)	-		2	Optimized according to clinical data		
Unbound fraction in gut	0.72	Assumed	1	Optimized according to clinical data		Same as TVR
Nominal flow in gut model (L/hr)	-		10	Optimized according to clinical data	-	
Distribution						
Distribution model	Full PBPK	Method 2	Minimal PBPK		Minimal PBPK	Same as TVR
Predicted Vdss (L/kg)	2.5	(Hyland et al., 2008)	2	Optimized according to clinical data	2	Same as TVR
Kp scalar	1.7	Adjusted to recover observed Vdss	-		-	
Elimination						
CYP3A4/5 CL$_{int,met}$ (mL/min/pmol)	44.6	(Tseng et al., 2018)	0.249	Optimized according to clinical data	-	
Another CL$_{int,met}$ (mL/min/pmol)	-		0.536	Optimized according to clinical data	-	
CL$_{int,HLM}$	-		-	-	33	Optimized according to clinical data
Microsomal protein binding (f$_{u,mic}$)	0.72	(Hyland et al., 2008)	1	Assumed	1	Assumed
Renal CL (L/h)	12	(Hyland et al., 2008)	-		-	

Enterohepatic circulation (%)	100	Assumed	-			
Transport						
Intestine						
$K_{m\ P\text{-gp}}$ (µM)	37	(Walker et al., 2005)	-			
$J_{max,P\text{-gp}}$ (pmol/min)	104	Measured	-			
Scaling factor	5	Optimized based on oral PK	-			
Liver						
PS_{pd} (mL/min/10^6 cells)	0.02	Measured	-			
$CL_{int,OATP1B1}$ (µL/m/10^6)	3.96	Measured	-			
Scaling factor	10	(Kimoto et al., 2017)	-			
$CL_{int,bile\ (P\text{-gp})}$ (µL/m/10^6)	2.4	Measured	-			
Interaction						
Enzymes						
CYP3A4 K_i (µM)	-		18.6	(INCIVEK (telaprevir))	18.6	(INCIVEK (telaprevir))
CYP3A4 K_I (µM)	-		2.24	Measured	-	
CYP3A4 K_{inact} (1/hr)	-		0.672	Measured	-	
Transporters						
P-gp K_i (µM)	-		0.48[†]	Optimized (see footnote)	0.48[†]	Same as TVR
OATP1B1 K_i (µM)	-		0.11[‡]	Optimized (see footnote)	0.11[‡]	Same as TVR

[*]Colonic absorption of MVC was assumed to be negligible (regional permeability of colon set as 0.01×10^{-4} cm/s).

[†]K_i value on P-gp was optimized to recover the TVR interactions with digoxin. This value is 10-fold lower than _in vitro_ K_i (4.8 µM) (Fujita et al., 2013).

[‡]K_i value on OATP1B1 was optimized to recover the TVR interactions with atorvastatin. This value is about 10-fold lower than the _in vitro_ K_i ($K_i = IC_{50}/2 = 1.1$ µM) (Kunze et al., 2012).

Table 2. Uptake of MVC, Pravastatin, Rosuvastatin and Propranolol by OATPs in Transfected HEK 293 Cells

Compound	Conc. (μM)	Uptake ratio		
		OATP1B1	OATP1B3	OATP2B1
MVC	0.1	3.1 ± 0.1	1.3 ± 0.1	1.2 ± 0.1
	1	2.5 ± 0.1	1.1 ± 0.0	1.0 ± 0.0
	10	2.2 ± 0.1	0.82 ± 0.02	0.81 ± 0.02
Pravastatin	1	64 ± 2	23 ± 1	2.1 ± 0.4
Rosuvastatin	1	95 ± 10	31 ± 2	19 ± 1
Propranolol	1	1.0 ± 0.1	0.64 ± 0.03	0.91 ± 0.04

The values are presented as uptake ratio (uptake by transfected cells over uptake by wild-type cells). The positive control substrates, pravastatin and rosuvastatin, and negative control, propranolol, exhibited uptake ratios of OATPs within the expected ranges. The uptake study was conducted with a substrate for 3 min. The values represent the mean ± S.D. (n = 3).

Table 3. PBPK Model Predictions of MVC Pharmacokinetics

Dose	Monitored	PK Parameters	Predicted	Observed	$R_{pred/obs}$	References for Observed
MVC						
Intravenous 3 mg	MVC	AUC_t (ng/mL/hr)	58.2	57.6	1.0	(Abel et al., 2008c)
		C_{max} (ng/mL)	34.3	36.9	0.94	
		CL (L/hr)	42.5	NC	-	
Intravenous 10 mg	MVC	AUC_t (ng/mL/hr)	230	201	1.1	(Abel et al., 2008c)
		C_{max} (ng/mL)	114	122	0.93	
		CL (L/hr)	42.5	NC	-	
Intravenous 30 mg	MVC	AUC_t (ng/mL/hr)	706	670	1.1	(Abel et al., 2008c)
		AUC_{inf} (ng/mL/hr)	717	687	1.0	
		C_{max} (ng/mL)	343	397	0.86	
		CL (L/hr)	42.5	44.0	0.97	
Oral 150 mg b.i.d.	MVC	$AUC_{t \, or \, inf}$ (ng/mL/hr)	542	599	0.90	(Vourvahis et al., 2014)
		C_{max} (ng/mL)	103	111	0.93	
		$F^{†}$ (oral 100mg)	0.17	0.23	0.72	(Abel et al., 2008c)
		$Fa \times Fg^{‡}$	0.44	0.71	0.61	
		$Fh^{††}$ (Intravenous 30 mg)	0.38	0.32	1.2	
TVR						
Oral 750 mg single	**TVR**	AUC_t (ng/mL/hr)	19421	11102-14930	1.3-1.7	(INCIVEK (telaprevir))
		C_{max} (ng/mL)	1861	1741-2217	0.84-1.1	
		T_{max} (hr)	4.88	4.0-5.0	0.98-1.2	
Oral 750 mg t.i.d.	**TVR**	AUC_t (ng/mL/hr)	26021	18850-20810	1.3-1.4	
		C_{max} (ng/mL)	3888	3104-3338	1.2-1.3	
		T_{max} (hr)	4.0	2.7-3.5	1.1-1.5	
	M0	AUC_t (ng/mL/hr)	15343	12320-14143	1.1-1.2	

		Cmax (ng/mL)	2099	1804-2076	1.0-1.2	
		Tmax (hr)	4.57	2.7-4.0	1.1-1.7	
Oral 750 mg t.i.d.	*TVR*	AUCt (ng/mL/hr)	20613	20013-21980	0.94-1.0	(Vourvahis et al., 2014)
		Cmax (ng/mL)	3236	3250-3533	0.92-1.0	
		Tmax (hr)	4.0	4.0	1.0	

NC, not calculated; F, oral bioavailability; Fa, fraction of the dose absorbed from gastrointestinal tract; Fg, fraction of the dose that escapes intestinal firs-pass metabolism; Fh, fraction of the dose that escapes hepatic firs-pass metabolism ; b.i.d., bis in die (twice a day); t.i.d., ter in die (three times a day)

[†]Predicted F was calculated by predicted AUC_{inf} *intravenous* 30 mg and *oral* 100 mg

[‡]Fa×Fg was calculated from F and intravenous CL (assumed to be hepatic CL, CLh), using expressions: F = Fa*Fg*Fh

[††]Fh was calculated hepatic CL, using $Fh = 1-CL_h/Q_h$; Q_h is hepatic blood flow. Non renal CL = 33.8 L/h at *intravenous* 30 mg from reference (Abel et al., 2008c) was used as CL_h.

Table 4. DDI Predictions of Probe Substrates with TVR

DDI with TVR	Elimination in model	Pred AUCR by HHEP-TDI	Pred AUCR by HLM-TDI	Obs AUCR (90% CI)	$R_{pred/obs}$ by HHEP-TDI	$R_{pred/obs}$ by HLM-TDI
Midazolam *Intravenous* 0.5 mg	CYP3A4, 3A5	4.55	12.6	3.4 (3.04, 3.79)	1.3	3.7
Midazolam *Oral* 2 mg	CYP3A4, 3A5	9.83	30.2	8.96 (7.75, 10.4)	1.1	3.4
Digoxin *Oral* 0.5 mg	P-gp (intestine, biliary)	2.14	-	1.85 (1.70, 2.00)	1.2	-
Atorvastatin *Oral* 20 mg	CYP3A (inh, TDI) OATP1B1 P-gp	14.0	29.0	7.88 (6.84, 9.07)	1.8	3.7

HHEP, human hepatocytes; HLM, human liver microsome; TDI, time-dependent inhibition; CI, confidence interval

Reference for Observed ACUR was (INCIVEK (telaprevir))

Simcyp default files for substrates were used; Sim-Midazolam and SV-Digoxin.

Table 5. DDI Predictions of MVC with Inhibitors and Inducers

MVC DDI with	Interactions in model	Pred AUCR	Obs AUCR (90% CI)	$R_{pred/obs}$	References for Observed
TVR 750mg t.i.d.	CYP3A (inh, TDI) OATP1B1 P-gp	7.90	9.49 (7.94, 11.34)	0.83	(Vourvahis et al., 2014)
Ketoconazole 450 mg q.d.	CYP3A (inh) P-gp	4.04	5.01 (3.98, 6.29)	0.81	(Abel et al., 2008b)
Ritonavir 100 mg b.i.d.	CYP3A (TDI, ind) P-gp	3.10	2.61 (1.92, 3.56)	1.1	(Abel et al., 2008b)
Efavirenz 600 mg q.d.	CYP3A (ind)	0.71	0.49 (0.41, 0.57)	1.4	(Abel et al., 2008a)
Rifampicin 600 mg q.d. [†]	CYP3A (inh, ind) OATP1B1 P-gp (ind)	0.37	0.33 (0.28, 0.38)	1.1	(Abel et al., 2008a)

CI, confidence interval; inh, inhibition; ind, induction; TDI, time-dependent inhibition; q.d., *quaque die* (once a day) ; b.i.d., *bis in die* (twice a day); t.i.d., *ter in die* (three times a day)

Simcyp default files for inhibitors were used; Sim-Ketoconazole-400mg QD, SV-Ritonavir, SV-Efavirenz and SV-Rifampicin-MD.

[†]SF for intestinal P-gp (x4) was assumed to induce P-gp in gut. The $K_{i,OATP1B1}$, CYP3A E_{max} and CYP3A EC_{50} values were used from the previous report (Varma et al., 2013).
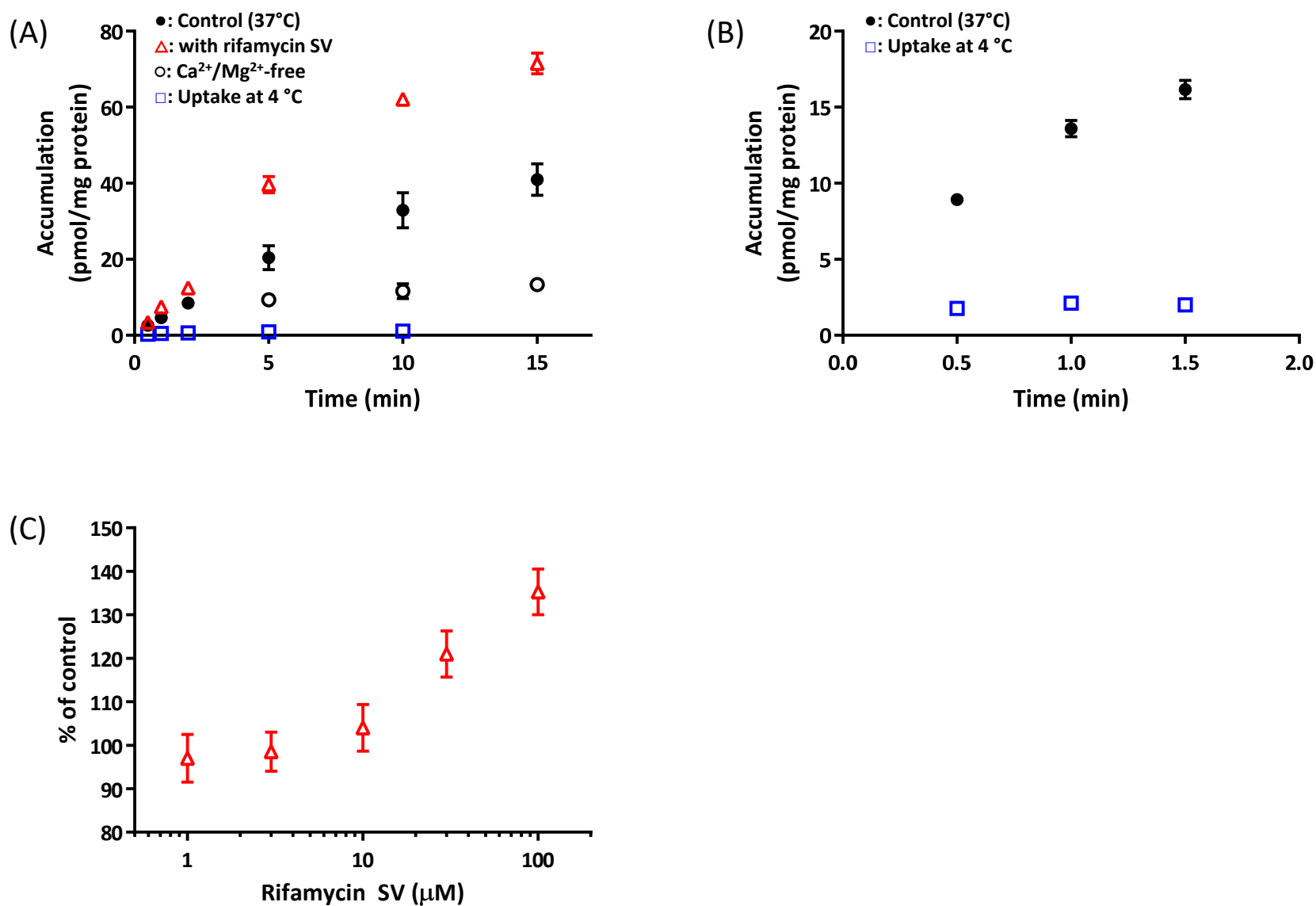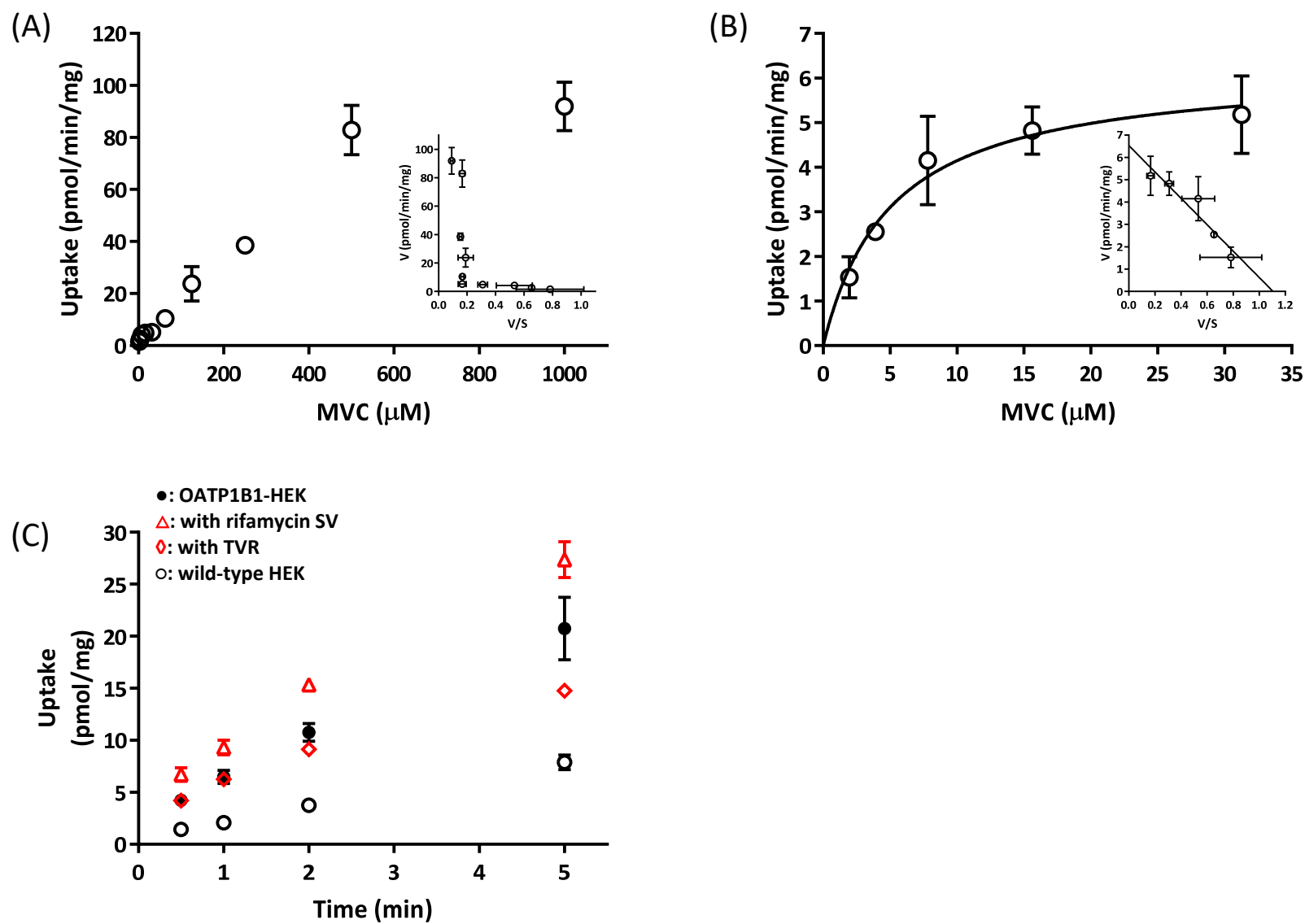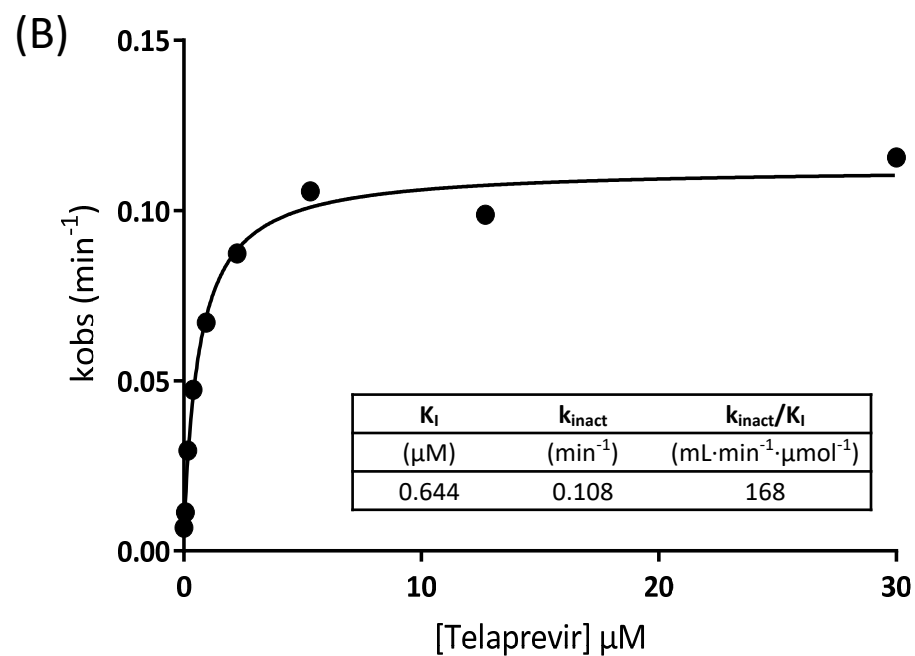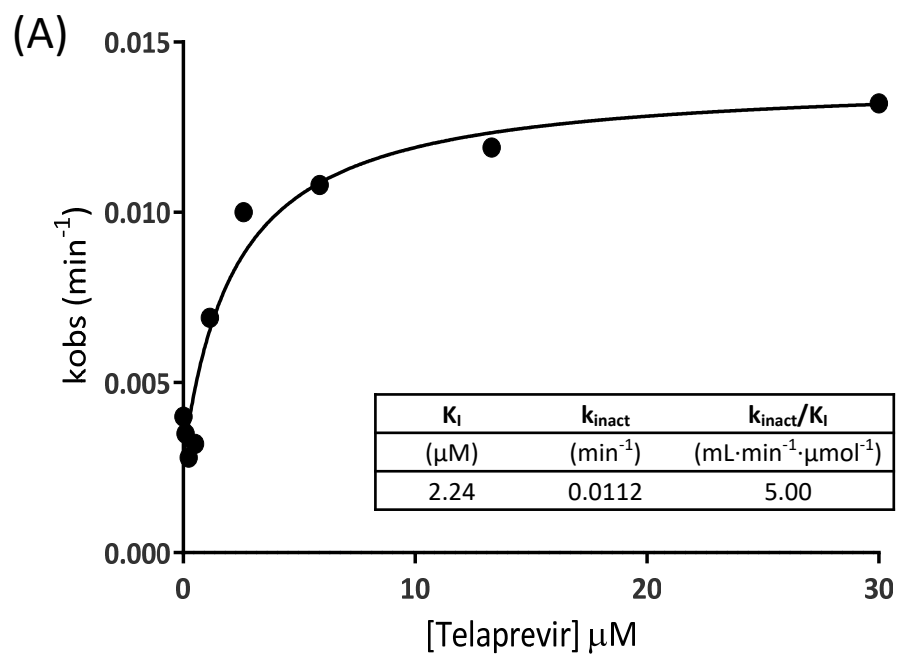
Figure 1

Figure 2

Figure 3

(A)

K_I	k_{inact}	k_{inact}/K_I
(μM)	(min^{-1})	(mL·min^{-1}·μmol^{-1})
2.24	0.0112	5.00

(B)

K_I	k_{inact}	k_{inact}/K_I
(μM)	(min^{-1})	(mL·min^{-1}·μmol^{-1})
0.644	0.108	168

Figure 4

(A)

(B)

(C)
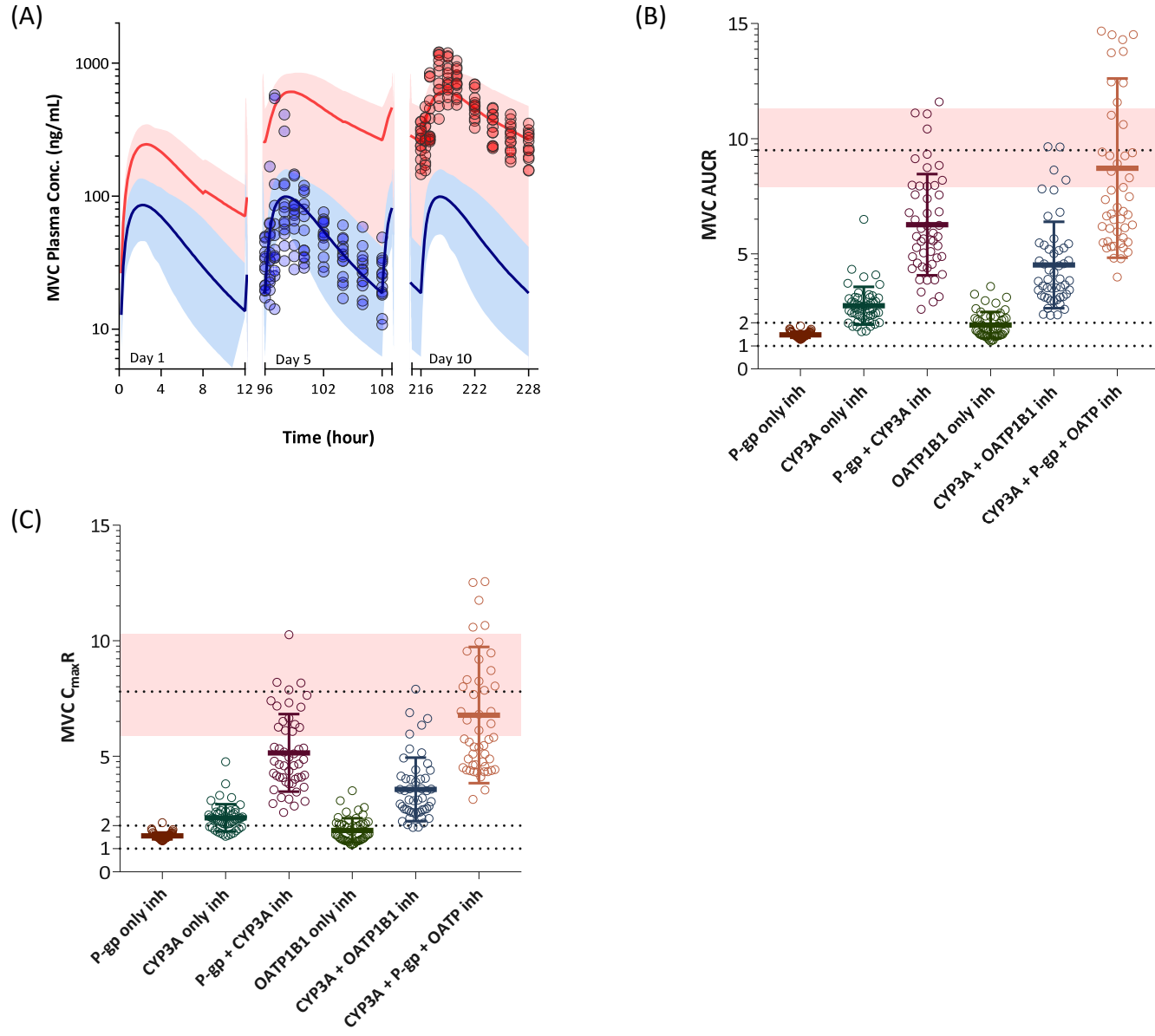
Figure 5
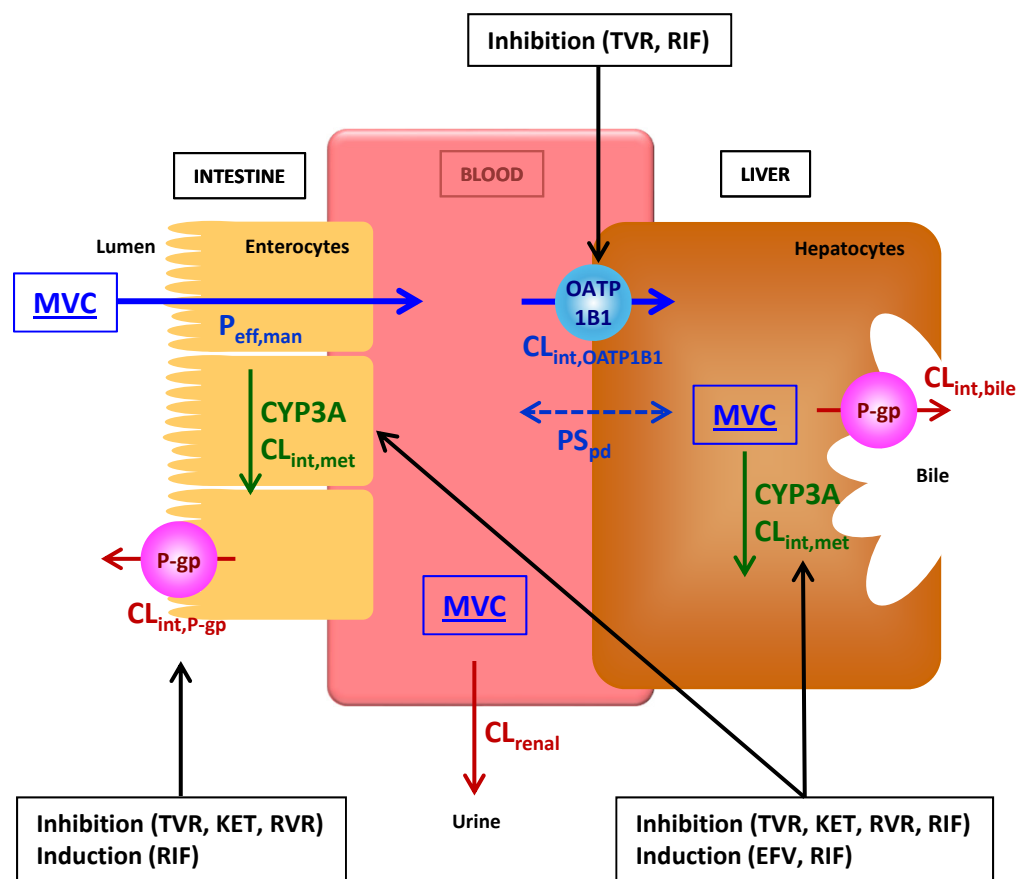
SUPPLEMENTAL DATA

Mechanistic Evaluation of the Complex Drug-Drug Interactions of Maraviroc: Contribution of Cytochrome P450 3A, P-Glycoprotein and Organic Anion Transporting Polypeptide 1B1

Emi Kimoto, Manoli Vourvahis, Renato J. Scialis, Heather Eng, A. David Rodrigues, Manthena V. S. Varma

Pharmacokinetics, Pharmacodynamics and Metabolism, Medicine Design, Pfizer Inc., Groton, CT, USA (EK, RJS[#], HE, ADR, MVSV); and Clinical Pharmacology, Pfizer Inc., New York, NY, USA (MV)

[#]Current affiliation: Metabolism and Pharmacokinetics, Preclinical Candidate Optimization, Bristol-Myers Squibb, Princeton, NJ, USA

Journal: *Drug Metabolism and Disposition*

The material includes one supplemental method and two supplemental figures.

Supplemental Methods

LC-MS/MS Analysis. MVC was analyzed on an API-4000 triple quadrupole mass spectrometer (Applied Biosystem, Foster City, CA) with an atmospheric pressure electrospray ionization source (MDS SCIEX, Concord, Ontario, Canada) that is connected to a SLC-20A LC system (Shimadzu, Kyoto, Japan) and HTC PAL autosampler (LEAP Technologies, Carrboro, NC). Samples (10 µL) were injected onto a Kinetex C18 column (2.6 µm, 100Å, 30 × 2.1 mm, Phenomenex, Torrance, CA) and eluted by a mobile phase with initial conditions of 10% solvent B, followed by a linear gradient of 10% solvent B to 90% solvent B over 1.5 min (solvent A: 100% water with 0.1% formic acid; solvent B: 100% ACN with 0.1% formic acid) at a flow rate of 0.5 mL/min. The mass-to-charge (m/z) transition in positive ion mode for monitoring MVC was m/z 514.6→280.2. Hydroxymidazolam was analyzed on a Sciex 6500 triple quadrupole mass spectrometer (Framingham, MA) fitted with an electrospray ion source operated in positive ion mode. An Agilent 1290 binary pump (Santa Clara, CA) with a CTC Leap autosampler (Leap Technology, Carrboro, NC) was programmed to inject 10 µL of sample on a Halo 2.7 µm C18 30 × 2.1 mm column (Advanced Materials Technology, Wilmington, DE). A binary gradient was employed using 0.1% formic acid in water (mobile phase A) and 0.1% formic acid in acetonitrile (mobile phase B) at a flow rate of 0.5 mL/min. Analytes 1'-hydroxymidazolam and D4-1'-hydroxymidazolam were monitored using multiple reaction monitoring mode for the m/z transitions 342.2 → 324.2 and 346.2 → 328.2, respectively.
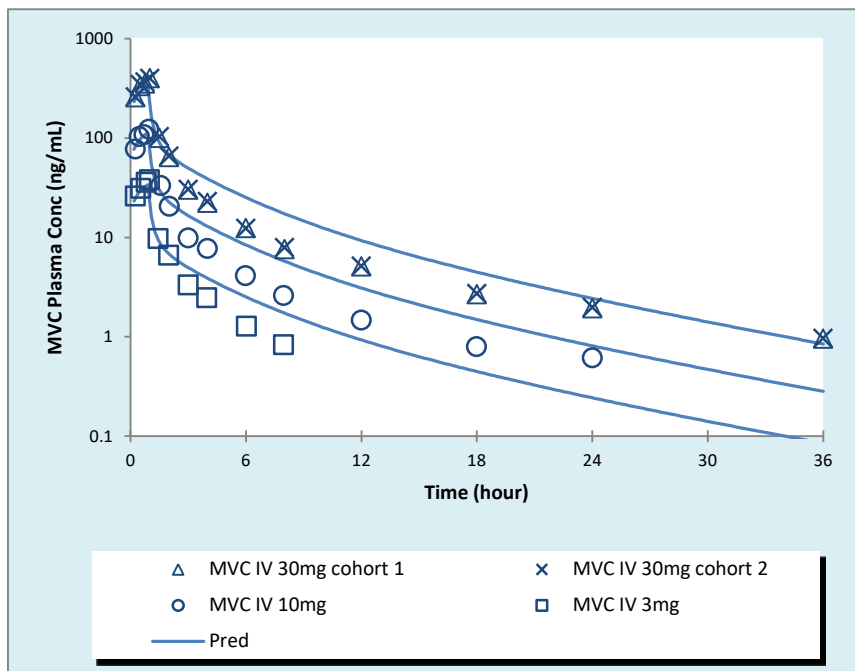
Supplemental Figures

Supplemental Figure 1A. Inactivation plots in hepatocytes to determine Kobs. Incubations were performed in duplicate, and individual activity values were plotted and analyzed.


% Remaining in human hepatocytes
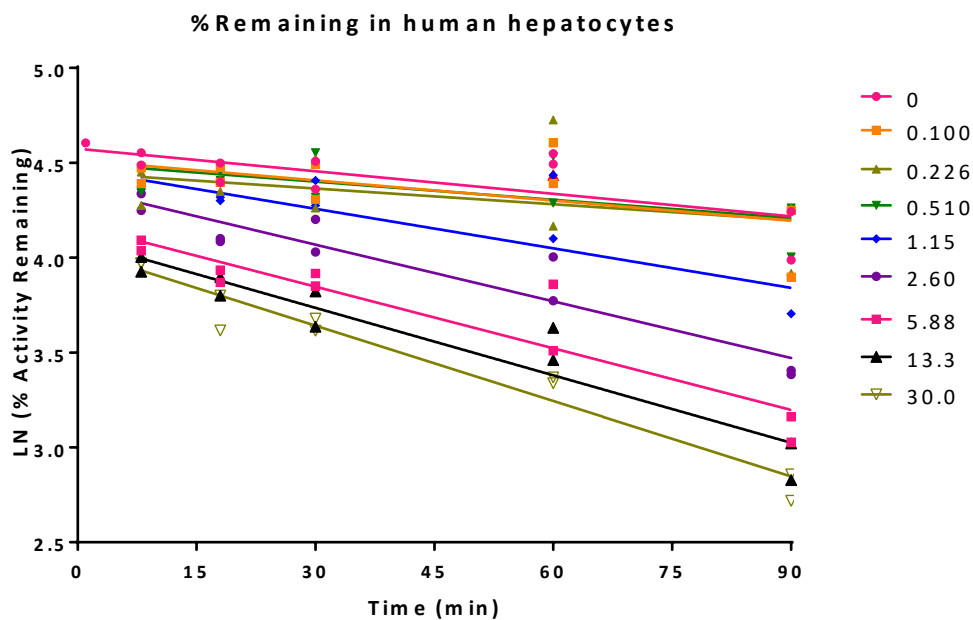
Supplemental Figure 1B. Inactivation plots in HLM to determine Kobs. Incubations were performed in duplicate, and individual activity values were plotted and analyzed. Experimental observations that were excluded from the kobs estimates are also indicated.

% Remaining in HLM
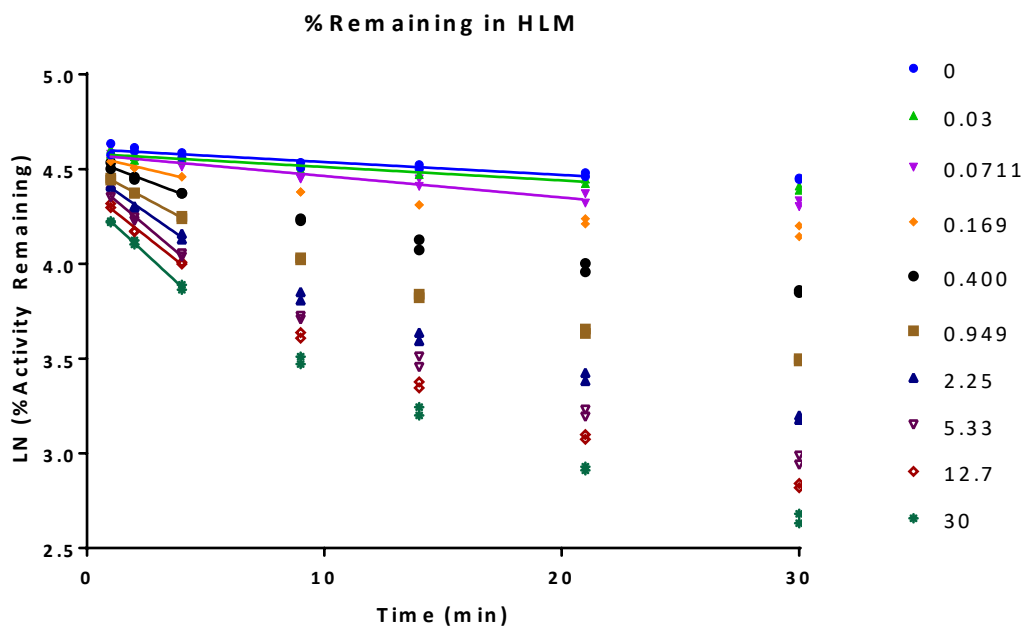
Supplemental Figure 2A. Simulated and Observed plasma concentration–time profiles of MVC following intravenous dose at 3 (□), 10 (○) and 30 mg (△ and ×). Solid lines (-) represents simulated data.

Supplemental Figure 2B. Simulated and Observed plasma concentration–time profiles of TVR following oral at single dose (○), multiple dose (△) in phase 1 studies and multiple dose in MVC-TVR DDI study (◇). Solid lines (-) represents simulated data.
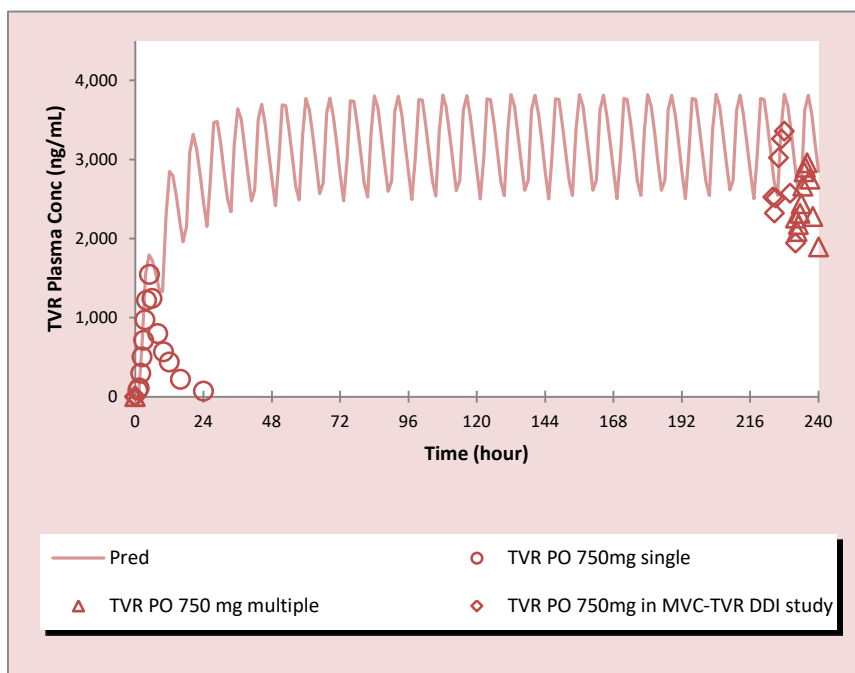
Supplemental Figure 3. Sensitivity analysis of K_i values for P-gp in gut and OATP1B1 in liver in MVC-TVR DDI prediction. Black arrow represents predicted AUC ratio with optimized K_i values of TVR for transporters. Red arrow represents predicted AUC ratio with original *in vitro* K_i values of TVR for transporters. Observed AUC ratio is 9.49 (90% confidence interval=7.94-11.34). Simulation results are based on 3 virtual trials of 3 subjects each to account for population variability.